Thermal structure and seismicity of subducting lithosphere

Brian Emmerson, Dan Mckenzie

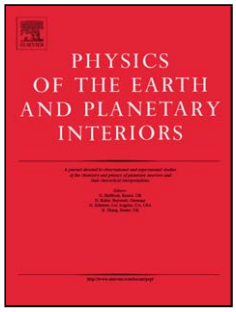

Title: Thermal structure and seismicity of subducting lithosphere

Authors: Brian Emmerson, Dan McKenzie

PII: S0031-9201(07)00104-5
DOI: doi:10.1016/j.pepi.2007.05.007
Reference: PEPI 4834

To appear in: *Physics of the Earth and Planetary Interiors*

Received date: 22-3-2007
Revised date: 11-5-2007
Accepted date: 12-5-2007

Please cite this article as: Emmerson, B., McKenzie, D., Thermal structure and seismicity of subducting lithosphere, *Physics of the Earth and Planetary Interiors* (2007), doi:10.1016/j.pepi.2007.05.007

Thermal structure and seismicity of subducting lithosphere

Brian Emmerson *, Dan McKenzie

Bullard Labs, Madingley Road, Cambridge, CB3 0EZ, UK

Abstract

It has recently been suggested that the mechanical behaviour of the oceanic and continental uppermost mantle depends on temperature alone, and that there is no strong evidence for compositional effects. It seems in the majority of cases that, if uppermost mantle temperatures exceed 600 °C, any deformation that occurs does so in the absence of significant seismicity. This observation apparently applies irrespective of whether that mantle material underlies an ocean or a continent. This paper investigates whether the same behaviour exists for earthquakes occurring in descending lithospheric slabs, namely whether there is some limiting temperature above which deformation occurs without significant seismicity, and whether that limiting temperature is consistent with the behaviour seen in the uppermost mantle beneath oceans and continents. By re-examining the thermal structure in subducting slabs, accounting for the temperature dependence of the relevant physical parameters, teleseismically-recorded seismicity is shown to be limited to material having *potential* temperatures less than $\sim$ 570–600 °C, or *homologous* temperatures less than ~ 0.42. The exceptions to this pattern occur in the subhorizontally subducting regions of the Nazca Plate, in which temperatures are probably affected by the relatively cold overriding plate.

Preprint submitted to Elsevier Science *11 May 2007*

Key words: Mantle rheology, seismicity, subduction zones, thermal modelling, potential temperature

1 Introduction

The tectonics and dynamic behaviour of the lithosphere are likely to be affected primarily by its composition and temperature structure. One obvious manifestation of these properties is the lateral- and depth-distribution of earthquakes. Oceanic plates as large as the Pacific Plate behave as rigid caps, transmitting stresses over large distances and concentrating deformation along their boundaries. Intraplate oceanic earthquakes occur in both the crust and the mantle (e.g. Wiens and Stein, 1983). In the continents, where deformation is more widely dispersed, the mantle is not a significant source of seismicity (Maggi et al., 2000b). Where oceanic lithosphere descends into the mantle at a subduction zone, earthquakes occur down to depths as great as 650–700 km (e.g. Frohlich, 2006). The primary factor controlling whether deformation is accommodated in a seismogenic, brittle fashion, or via some form of aseismic creep is thought to be temperature. Knowledge of lithospheric temperature structure comes from simple thermal models describing geophysical observables such as topography, bathymetry, seismic velocity, and heat flow, and geological data such as the composition of exhumed rocks. Improvements in experimental data further constrain these models, refining the understanding of what controls lithosphere rheology. This paper investigates

* Corresponding author
Email address: emmerson@esc.cam.ac.uk (Brian Emmerson).

the effect such improvements have on understanding thermal controls on deep seismicity in subduction zones, and whether these controls fit with what is currently known about the earthquake distribution in oceanic and continental lithosphere.

The plate model of oceanic lithosphere formation and cooling (McKenzie, 1967; Parsons and Sclater, 1977) has proven remarkably successful in explaining the observed variation of heat flow and bathymetry with the age of the ocean floor. Furthermore, the model suggests that there exists a limiting temperature in oceanic lithosphere, above which significant earthquakes (those with $M_w \gtrsim 5$) do not occur (Wiens and Stein, 1983). However, studies of continental earthquake focal depths have shown that almost all continental events occur in the crust, and that the continental mantle is almost entirely aseismic (Jackson et al., 2004; Maggi et al., 2000b; Mitra et al., 2005). Where the lower crust is seismically active (e.g. east Africa, north India), Maggi et al. (2000b) found that the uppermost mantle was not; even though the Moho temperature in these places was thought to be as low as 400–500 °C. Since earthquakes were thought to occur in mantle material with temperatures up to 750 °C in the oceans (Chen and Molnar, 1983; Wiens and Stein, 1983), some explanation other than temperature was necessary to explain the lack of mantle seismicity in these continental areas. Maggi et al. (2000a) suggested that the lack of significant continental seismicity deeper than the Moho was due to the weakening of the mantle by water, contained in hydrous minerals. While this is plausible, a simpler explanation has since been proposed by McKenzie et al. (2005), who concluded that continental Moho temperatures in these areas were underestimated, and that temperatures in the middle of oceanic plates were overestimated.

The analytic plate-cooling model for oceanic lithosphere assumes that the thermal conductivity, thermal expansivity, specific heat capacity, and initial (midocean ridge) temperature are all constant. These assumptions are known to be incorrect. Experimental work has constrained variations in the relevant physical parameters with temperature, and the temperature at both the base of the plate and the ridge axis are constrained by the requirement that, away from plumes and fracture zones, an oceanic crustal thickness of 7.1 ± 0.8 km be produced by isentropic upwelling at midocean ridges (White et al., 1992). Also, shear wave velocity variations beneath the oceanic plates indicate variations in temperature that are smaller than a few tens of °C (Priestley and McKenzie, 2006). McKenzie et al. (2005) have shown that a modified plate-cooling model incorporating these restrictions can explain the observed variations in heat flow and bathymetry at least as well as an analytic model with constant and adjustable coefficients. The most significant feature of their model is that the central portion of the plate is cooler than in the analytic case, in agreement with the results of Honda and Yuen (2001), who found that a model incorporating variations in the conductivity and expansivity results in a colder modelled plate interior. Such a colder interior is due mainly to the decrease of thermal conductivity with increasing temperature, and suggests that the majority of intraplate oceanic earthquakes occur in material having a temperature less than 600 °C (McKenzie et al., 2005). Furthermore, by reassessing steady state continental geotherms used to fit thermobarometric estimates from mantle nodules, McKenzie et al. (2005) also showed that, if heat production throughout the continental crust is taken into account, Moho temperatures in the ancient Precambrian shields are likely to be between 500 and 600 °C (e.g. Emmerson et al., 2006). The paucity of recorded seismicity in the continental mantle can also, therefore, be explained in terms of tem-

perature. McKenzie et al. (2005) point out that, although earthquakes with magnitude ~ 5.5 or greater may occur below the Moho if the mantle is colder than $\sim 600\,^{\circ}\mathrm{C}$, they are rare and none have yet been detected. The observed pattern of seismicity in the uppermost mantle beneath the oceans and the continents therefore appears to be controlled by temperature alone. This paper aims to determine whether the same is true for the distribution of subduction zone earthquakes.

Almost all deep seismicity (events with depths > 60 km, which account for approximately a quarter of all earthquakes) occurs within relatively cold, oceanic lithosphere as it descends into the mantle at subduction zones. The first estimation of the temperatures above which earthquakes cease to occur was performed by McKenzie (1969), who used an analytic model to estimate the depth to which a given isotherm penetrates. He concluded that a temperature of $\sim 680\,^{\circ}\mathrm{C}$ limits the down-dip extent of earthquakes, but subsequently showed that, because of the isentropic increase of temperature with depth in the mantle, this is in fact a limiting *potential* temperature (McKenzie, 1970). Molnar et al. (1979) examined a large number of subduction zones, and showed an absence of seismicity at potential temperatures exceeding $\sim 630\,^{\circ}\mathrm{C}$. Subsequently, Wortel (1982) and Wortel and Vlaar (1988) applied the same modelling technique and showed that the deepest seismicity in subduction zones is limited to material having a homologous temperature between $\Theta \approx 0.40$–0.50 (where the homologous temperature Θ is defined as the ratio of the Kelvin temperature to the Kelvin melting temperature). More recently, thermal models of subduction zones have incorporated advection of heat via circulation in the mantle wedge (e.g. England and Wilkins, 2004; van Keken, 2003). In light of what is now known about plate ages and thicknesses, the temperature de-

pendence of the relevant physical parameters, the background temperature of the upper mantle, and the improved knowledge of earthquake hypocentral locations provided by the EHB catalogue (Engdahl et al., 1998), it is worthwhile to reassess the (potential and homologous) temperatures above which deep earthquakes cease to occur. Such a reassessment seems particularly relevant in light of the lower temperatures obtained for the interiors of oceanic plates by incorporation of temperature-dependent physical parameters in the thermal model, and the subsequent impact on reconciling the distribution of intraplate seismicity in the uppermost oceanic and continental mantle (McKenzie et al., 2005). This investigation is not concerned with the mechanism through which deep earthquakes occur, about which there has been much debate (e.g. Frohlich, 2006). Instead, it is concerned with the temperatures above which deformation, however it occurs, ceases to be seismogenic, and whether these temperatures are in agreement with the pattern of seismicity seen in the uppermost mantle beneath the oceans and the continents. Without the detailed modelling using the improved data outlined above, with which this paper is concerned, it is not obvious on which variant of temperature — be it Celsius, potential, or homologous temperature — that the material properties of subducting lithosphere depend, or indeed if the seismicity contained therein can be described by a limiting temperature at all.

In this paper, numerical modelling used to determine temperatures in subducting slabs, incorporating the temperature dependence of the relevant physical parameters, is outlined. Following this is a description of the methods of data analysis and a comparison between the Celsius temperatures, potential temperatures, and homologous temperatures at which the deepest earthquakes occur in each region, for a variety of models. The paper finishes with a dis-

cussion of results that are less well constrained, including the effects shallow dips of subduction may have on the thermal structure in descending slabs.

2 Modelling the thermal structure of subducting slabs

The thermal structure of sinking oceanic lithosphere was first modelled by McKenzie (1969), who treated the subducting plate as a two dimensional rigid slab of thickness a, descending at speed v into a mantle of constant temperature T_1. Using a constant conductivity k, specific heat capacity C_P, and density ρ, he obtained an analytic expression for the temperature variation within the slab as a function of down-dip distance x. Subsequently, it was argued that, because of the approximately isentropic increase in temperature with depth in a vigorously convecting mantle, the contours of temperature obtained by McKenzie (1969) were in fact contours of *potential* temperature T_p (McKenzie, 1970). The analytic expression of McKenzie (1969) assumes that the temperature structure of the slab entering the trench is that of a thermally equilibrated cooling oceanic plate. In practice such a temperature structure is appropriate for plates whose age exceeds $\sim 2\tau$, where $\tau = a^2/\pi^2\kappa$ ($\kappa \equiv k/\rho C_P$). For oceanic plates, $\tau \sim 60$ Myr. Molnar et al. (1979) applied McKenzie's analytic expression for potential temperature to several subduction zones, but estimated the effective thickness (a) of the oceanic lithosphere entering the trench, defining the plate thickness to be the depth at which linear extrapolation of the surface temperature gradient intersects the temperature profile of the convecting mantle. In this way, Molnar et al. incorporated into their modelling the effect the age of oceanic plate entering the trench (A_{trench}) has on the temperature structure at depth. Using values of

$k = 3.0\ \mathrm{W\,K^{-1}\,m^{-1}}$, $\rho = 3350\ \mathrm{kg\,m^{-3}}$, $C_P = 1000\ \mathrm{J\,K^{-1}\,kg^{-1}}$, and thermal expansivity $\alpha = 3.0 \times 10^{-5}\ \mathrm{K^{-1}}$, they found no earthquakes occurring in subducting slabs with potential temperatures exceeding $\sim 630\,^{\circ}\mathrm{C}$, for a mantle with a background $T_p = 1200\,^{\circ}\mathrm{C}$.

The dependence of thermal conductivity k on temperature has a significant effect on the temperature structure of a cooling oceanic plate (McKenzie et al., 2005). Experimental work by Schatz and Simmons (1972) shows that, in the temperature range applicable to cooling and subducting oceanic plates ($\sim$ 0–1500 °C), k varies by a factor of about two. Using temperature-dependent physical parameters $k(T)$, $\alpha(T)$, $\rho(T)$, and $C_P(T)$, as well as a background mantle potential temperature required to produce an oceanic crust 7 km thick by decompression melting, the only remaining adjustable parameter in plate models of oceanic bathymetry and heat flow is the plate thickness a. Despite this restriction, McKenzie et al. (2005) were able to produce an equally good fit to the bathymetric and heat flow data from the north Pacific as Parsons and Sclater (1977), who used adjustable, constant values of a, T_1, k, and α to fit the same data. However, temperatures in the middle of the oceanic plate are significantly cooler in the model of McKenzie et al. (2005), and consequently the temperatures up to which the earthquakes are estimated to occur are about 100 °C lower.

In the absence of shear heating, the steady-state advection-diffusion equation for a compressible material having temperature-dependent density $\rho(T)$, specific heat capacity $C_P(T)$, and conductivity $k(T)$ is

$$\rho(T)C_P(T)\mathbf{v}\cdot\{\nabla T - (\nabla T)_S\} = \nabla\cdot\{k(T)\nabla T\} + H, \qquad (1)$$

where $\mathbf{v}$ is the material velocity, and a subscript S denotes variations in T due to isentropic compression or expansion. The concentrations of uranium, thorium, and potassium in the upper mantle are low enough to allow the rate H of radiogenic heat production per unit volume to be ignored. Furthermore, in subducting slabs down-dip heat transport is dominated by advection, meaning down-dip heat conduction can be ignored and the temperature $T = T(x, y)$ in the coordinate system illustrated in Fig. 1(i) is given by

$$\rho(T)C_P(T)v\left\{\frac{\partial T}{\partial x} - \left(\frac{\partial T}{\partial x}\right)_S\right\} = \frac{\partial}{\partial y}\left(k(T)\frac{\partial T}{\partial y}\right), \tag{2}$$

since the plate velocity $\mathbf{v} = (v_x, v_y) = (v, 0)$. For a slab of thickness a dipping at an angle δ, as shown in Fig. 1(i), the depth of a point (x, y) is $z(x, y) = a(1-\cos\delta) + x\sin\delta + y\cos\delta$. The isentropic variation of temperature with down-dip distance x can therefore be written in terms of the isentropic variation of temperature with depth z via

$$\left(\frac{\partial T}{\partial x}\right)_S = \frac{\partial z}{\partial x}\left(\frac{\partial T}{\partial z}\right)_S = \sin\delta\left(\frac{\partial T}{\partial z}\right)_S. \tag{3}$$

[Fig. 1 about here.]

For the Earth, the following holds to good approximation:

$$\left(\frac{\partial T}{\partial z}\right)_S = \frac{\alpha(T)g}{C_P(T)}T. \tag{4}$$

If the integral

$$G = \int k(T)\mathrm{d}T \tag{5}$$

can be obtained, Eqs 2–5 can be combined to give the equation describing variations in temperature within the frame of the plate:

$$\frac{\partial T}{\partial t} \equiv v\frac{\partial T}{\partial x} = \frac{1}{\rho(T)C_P(T)}\frac{\partial^2 G}{\partial y^2} + \frac{vg\alpha(T)\sin\delta}{C_P(T)}T. \tag{6}$$

By ignoring the second term on the right hand side, the effect of the diffusion term in Eq. 6 is obtained using the generalised Crank-Nicolson numerical scheme from Press et al. (1992, p.842). Details of this implementation are given by McKenzie et al. (2005, their Eq. 11).

By ignoring the first term on the right hand side of Eq. 6, it can be rewritten as:

$$\int_{T_j^n}^{T_j^{n+1}} \frac{C_P(T)}{gT\alpha(T)\sin\delta}\mathrm{d}T - \Delta t = 0. \tag{7}$$

Simpson's rule was used to evaluate the integral, and the root T_j^{n+1} that satisfies Eq. 7 was determined by iteration. The full solution to Eq. 6 was produced using the operator splitting method described by Press et al. (1992, p.847), substituting the solution T_j^{n+1} from Eq. 11 in McKenzie et al. as the value of T_j^n in Eq. (7). The accuracy of the numerical scheme was tested for the subducting plate by comparison with the analytic solution (McKenzie, 1970), using $G = kT$ (where k is the constant value of the conductivity) and constant values of α, ρ, and C_P. For a plate speed $v = 75$ mm yr^{-1}, the root mean square error was less than 5 °C.

For thermal modelling in which $k = k(T)$, the expression for conductivity used by McKenzie et al. (2005, their Eq. 4) was adopted, which is integrable and differs from that proposed by Hofmeister (1999) by less than the standard deviation of the experimental data (Schatz and Simmons, 1972) in the temper-

ature range of interest. The experimental data of Schatz and Simmons, along with the parametrisation employed here, are in excellent agreement with the diffusivity data and parametrisations of Pertermann and Hofmeister (2006). For self consistency, variations of α, ρ, and C_P with temperature are included, though the effects such variations have are small compared with the effect of temperature on conductivity. The parametrisation of $\alpha(T)$, $\rho(T)$, and $C_P(T)$ employed is identical to that given in McKenzie et al., their Eqs 8–10. [The thermal expansivity is parametrised as in Eq. 8 of McKenzie et al. (2005), with $\alpha(T) = \alpha_0 + \alpha_1 T$. However, the printed value of α_1 in Eq. 8 of McKenzie et al., is incorrect. The correct value, used both here and in their calculations, is $\alpha_1 = 7.58 \times 10^{-9}$ K^{-2} (Bouhifd et al., 1996).]

When the heat capacity and thermal expansivity are treated as constant, Eq. 4 is trivially integrated and temperature is related to potential temperature T_p by a simple exponential, $(T + T_0) = (T_p + T_0) \exp(\alpha g z / C_p)$, where T is the Celsius temperature and $T_0 = 273$ K. For models where α and C_P vary with temperature, conversions were made between temperature and potential temperature by integrating Eq. 4 numerically. The potential temperature of the mantle was chosen to be 1315 °C, which generates a crustal thickness of 7 km by decompression melting when the entropy of melting ΔS is 400 J K^{-1} kg^{-1} (Kojitani and Akaogi, 1997).

Input thermal structures $T(x, y) = T(0, y)$ for the subducting slab were taken from the plate-cooling models of McKenzie et al., which give the temperature $T_{cool}(A, z)$ of a cooling plate of constant thickness as a function of plate age A. The effect that the age of material currently entering the trench (A_{trench}) has on slab thermal structure was accounted for using the temperature profile $T_{cool}(A_{trench}, z)$ as the initial profile $T(0, y)$ of the subducting plate (Fig. 1).

For the subduction stage of the plate's thermal history, the upper boundary condition $T(0,0)$ was changed from the zero temperature used for the cooling stage to the isentropic temperature at depth $z = a(1-\cos\delta)$ (Fig. 1(i)). The effects of using temperature-dependent versus constant physical parameters were compared, as well as the effect that different temperature structures, applied to the upper and lower slab surfaces, have on the resulting temperatures within the slab itself. Temperatures on $y = 0, a$ were set in two ways. First, the potential temperature on the slab surfaces was fixed so that the temperatures $T(x,0)$ and $T(x,a)$ increase isentropically according to Eq. 4 as the slab descends deeper into the mantle. These boundary conditions assume that circulation in the surrounding mantle advects cold material away from the slab boundaries with sufficient vigour to keep them at the same potential temperature as the convecting background mantle. Secondly, we investigated how conductive cooling of mantle material adjacent to the slab affects temperatures in the slab interior. In this case, the initial temperature structure $T(0,y)$ at the onset of subduction was set up by embedding $T_{cool}(A_{trench}, z)$ in the background isentropic gradient of the mantle, as shown in Fig. 1(ii). This three-layered system, comprising the initially hot mantle above the slab, the relatively cold slab itself, and the initially hot mantle below the slab, was then evolved according to Eq. 6. By embedding the slab in a background mantle temperature gradient at the onset of its descent into the mantle and allowing that three-layered system to evolve over time, we effectively fix the potential temperature of the mantle far from the slab surface, allowing investigation of the effects of conductive cooling in the mantle immediately adjacent to the slab on temperatures in the slab itself. This approach is qualitatively similar to that proposed by Davies (1999). Conductive cooling in the chosen Lagrangian reference frame ignores relative motion between the slab and

surrounding mantle, and as such neglects advective transport of heat (as measured in the plate's frame of reference) in the layers above and below the slab. However, these sets of boundary conditions describe the two end members in 1D models of cooling plates: in the first case, mantle adjacent to the plate convects with sufficient vigour to rapidly remove conductively cooled material; in the second, no cooled material is removed.

Contours of Celsius temperature in subducting slabs with different modelling parameters are shown in Fig. 2, which illustrates the effects of using temperature-dependent versus constant k, α, ρ, and C_P, as well as the effect of allowing the mantle adjacent to the subducting slab to cool conductively. Each figure shows a slab of thickness a (outlined, dashed line) descending with a dip $\delta = 45°$ and speed $v = 75$ mm yr^{-1} into an isentropic mantle temperature gradient with $T_p = 1315\,°\mathrm{C}$ (oblique lines seen for $y < 0$ and $y > a$). The input temperature $T(0, y)$ is that of a 50 Myr old plate of thickness $a = 106$ km (Fig. 1(ii)). Comparison of Fig. 2(i) (constant physical properties) with Fig. 2(ii) (variable physical properties) shows that, because the conductivity and, as a result, the diffusivity $\kappa \equiv k/\rho C_P$, decrease with temperature, temperature differences between the slab interior and its surroundings can be maintained for longer periods when $k = k(T)$, meaning that the plate interior is cooler than for the situation with a constant diffusivity. This is despite the slightly hotter isentropic temperature profile with depth produced by the temperature-dependent thermal expansivity and heat capacity employed here. Wortel (1982) found that results modelled using a constant diffusivity did not differ significantly from those determined from a conductivity with a temperature dependence based on the same experimental data as that used here (Schatz and Simmons, 1972). These results are discussed further in §5. A slab surrounded by a man-

tle that is allowed to cool conductively has a cooler interior (Fig. 2(iii)) than a slab having boundaries that are fixed at a constant potential temperature (Figs 2(i) and (ii)). For most situations encountered, the subduction stage is not strongly affected by the use of different, physically reasonable mid-ocean ridge temperature structures at the onset of the plate-cooling stage, and the effects of such different structures on the subducting slab decrease with increasing A_{trench}. Subducting slab temperature structures for two different ridge temperature structures are compared in Fig. 2(ii) (see dotted lines).

[Fig. 2 about here.]

3 Subduction zones of the world

In order to estimate the temperatures above which earthquakes cease to occur in subducting oceanic lithosphere, profiles through deep and intermediate-depth hypocentres from the updated catalogue of Engdahl et al. (1998, the "EHB" catalogue) were analysed. Arc-perpendicular profiles through the seismicity were constructed using the technique of England et al. (2004), with hypocentres within a swath ±150–200 km wide projected onto each profile. Profiles analysed in this paper are summarised in Table 1 and shown in Fig. 3. The dip δ of the Wadati-Benioff zone was measured by fitting, by eye, a linear trend to events deeper than 80 km. Lengths L of the seismic part of the slab were obtained by projecting this linear fit up to the surface, and measuring the distance along the trend line from the surface to the deepest seismicity. Measurements of slab dip made by eye are less sensitive to outliers than are automated fitting routines, and by fitting manually it was possible to account for dips that change significantly along the length of the seismic zone. In re-

gions where the dip shallowed or steepened significantly along a given profile (e.g. Java), the steeper dip was used, but the seismic slab length was measured in separate stages along the whole Wadati-Benioff zone. Errors in the dip estimates are likely to be less than $\pm 5^{\circ}$. In the Pampean (symbol $\odot$) and Peruvian ($\oplus$) regions of the subducting Nazca Plate, the localised clusters of events at depths $z > 500$ km were ignored. These events are isolated from the subhorizontally dipping seismicity at shallower ($z < 200$ km) depths, and were interpreted as occurring within detached portions of subducting lithosphere. Results are only presented for profiles whose deepest events exceed depths of 150 km, as the slab geometry is generally poorly defined if the deepest seismicity is shallower than this. Furthermore, for slabs where the deepest earthquakes lie at such shallow depths, the temperature structure in the subducting plate is likely to be dominated by the effect of the overriding plate.

[Table 1 about here.]

[Fig. 3 about here.]

3.1 Plate ages

Ages of material presently entering the trench (A_{trench}) and estimated errors associated with those ages were taken from the age and age error grids of Müller et al. (2006). Errors in age estimates have a larger effect on the modelled temperature structures for younger values of A_{trench}. For regions (Ryukyu, Aegean) where no or only partial age information was available from Müller et al. (2006), either the age information available for that region was interpolated (Ryukyu), or an alternative estimate of A_{trench} was used (Ken-

nett, 1982, Aegean), with an error of ±15 Myr arbitrarily assigned in each case.

Molnar et al. (1979) assumed that, for most of the world's subduction zones, the age of the subducted lithosphere has been approximately constant for the past ∼ 10 Myr, based on the fact that the age of sea floor increases towards the arc, and that present rates of seafloor creation and subduction are comparable. For the portion of oceanic lithosphere currently present at the tip of a seismically active region of length L', the age A_{tip} of that material at the time when it first entered the trench was estimated from

$$A_{tip} = A_{trench} + \left(\frac{\mathrm{d}A}{\mathrm{d}r} - \frac{1}{v_\perp} \right) L', \tag{8}$$

where $v_\perp$ is the arc-perpendicular convergence rate, and r is the distance measured in the same direction as $v_\perp$. For each profile, A_{tip} was estimated using $L' = L$, the length of the seismic zone. Approximate errors in tip ages were estimated by considering the range of A_{tip} values produced by Eq. 8 using a linear weighted least-squares fit to the available age data for 150 km $\leqslant L' \leqslant L$. Values of A_{tip} calculated in this way are mainly smaller than values of A_{trench} (Table 1).

3.2 Convergence rates

In the absence of significant shortening in the forearc, arc-perpendicular convergence rates ($v_\perp$) between a subducting and overriding plate are equal to the rate at which the subducting plate descends into the mantle (v in Eq. 1). Convergence rates were calculated by projecting onto the profile in question

the plate-relative-velocity vectors determined at the trench. In most cases, relative velocities were calculated using NUVEL-1A (DeMets et al., 1994). For the Aegean, the Aegean-Eurasian angular velocity (Le Pichon et al., 1995) was combined with the NUVEL-1A Africa-Eurasia angular velocity to calculate the convergence rate. The angular velocity of convergence for the Windward and Leeward Islands was taken from DeMets et al. (2000). Estimates of Philippine Sea Plate motion based on inversions of earthquake slip vector data are poorly constrained (Seno et al., 1993), hence for arcs bordering the Philippine Sea the geodetically determined poles of rotation (Sella et al., 2002) were used to determine the overall plate motion. Errors in all convergence rates were calculated from rotation pole error ellipses.

3.3 Backarc spreading

Backarc spreading increases the arc-perpendicular convergence rate for a subduction zone, though the effect on thermal structure is not well known. Because of uncertainties about its history, in regions where backarc spreading is significant (S. Sandwich, Mariana, Tonga, Kermadec) results are compared using convergence rates that both include (flagged "B" in Table 1) and exclude it. By treating as separate the plates either side of the spreading centre behind the South Sandwich arc, the pole of relative rotation between the Sandwich Plate and the South American Plate (Thomas et al., 2003) includes the effects of spreading in the Scotia Sea; the Scotia Plate-South American Plate pole excludes it. Jarrard (1986) used marine magnetic anomalies spanning the past 2–7 Myr to argue that full spreading rates for the Mariana, Tonga, and Kermadec arcs are 43 mm yr^{-1}, 50 mm yr^{-1}, and 54 mm yr^{-1} respectively. Backarc

spreading was included in these three regions by adding the full spreading rates to the arc-perpendicular convergence rates.

3.4 Results classification

The subduction zones studied divide into two types, grouped here under "class 1" or "class 2." The former are simple ones where the present subduction rate is well determined, because the plates involved are so large and their relative motion is unlikely to have changed significantly over the past few Myr. The latter involve motion between plates whose velocities, and especially the histories of the velocities, are poorly known, either because of backarc spreading, or because, like the Philippine Sea Plate, they are surrounded by subduction zones. In addition, the Aegean is included as a class 2 region because the age of subducting material is poorly known. Class 1 results provide the better test of the model outlined in §2.

4 Deepest seismogenic temperatures

At the maximum down-dip extent $x^\star$ of a given isotherm within a subducting slab, the temperature gradient $(\partial T/\partial y)_{x=x^\star}$ is zero (Fig. 2). The difference between the depth to which that isotherm penetrates and the point $z^\star \equiv z(x^\star, y)$ is unimportant. Hence, if the deepest earthquake in a profile had a depth z_d, the temperature of the slab at that depth was estimated by equating $z^\star$ to z_d, and calculating the temperature for the determined slab dip, age, and convergence rate. The Celsius temperature T_d at the depth of the deepest teleseismically-recorded earthquake is referred to below as the "deepest seis-

mogenic temperature," and the equivalent potential temperature the "deepest seismogenic potential temperature," $T_{p,d}$. "Deepest seismogenic homologous temperatures," Θ_d, are defined as $\Theta_d \equiv \frac{T_d+T_0}{T_m(z_d)+T_0}$, where $T_m(z_d)$ is the Celsius melting temperature at depth z_d and $T_0 = 273$ K. The solidus temperature of anhydrous peridotite, as parametrised by Zhang and Herzberg (1994), was taken as the value of T_m, and the resulting values of Θ_d are denoted by an additional subscript ZH as $\Theta_{ZH,d}$. Estimates of the deepest seismogenic temperatures of course assume that the deepest recorded earthquakes in a region are representative of the deepest seismicity in that region over several tens or hundreds of thousands of years. In regions where seismicity is frequent and the seismogenic slab is clearly delineated by earthquake hypocentres, this assumption is likely to be accurate. However, where seismicity in the subducting slab is sparse (e.g. S. Chile), the deepest earthquakes catalogued to date may not be representative of the longer-term deepest seismicity.

Calculated values of T_d or $T_{p,d}$ as a function of z_d for a range of modelling parameters are shown in Figs 4–8, with data points labelled according to region. Depths z_d to the deepest earthquakes are assigned a constant error of $\pm$20 km, based on discrepancies between local and teleseismic locations (e.g. Engdahl et al., 1998; England et al., 2004). Bounds on T_d and $T_{p,d}$ were determined from errors in the values of $v_\perp$ and A_{trench}. Minimum values for T_d and $T_{p,d}$ shown in Figs 4–8 were calculated by combining the maximum calculated value of $v_\perp$ with the maximum estimated value of A_{trench}; maximum values were calculated combining the minimum $v_\perp$ with the minimum A_{trench}. Class 1 results and class 2 results are shown in Figs 4–7 and Fig. 8 respectively, and homologous temperatures modelled for class 1 results are shown in Fig 9.

Figure 4 shows deepest seismogenic temperatures estimated for class 1 re-

sults (Table 1), using the best-fitting constant physical parameters determined by Parsons and Sclater (1977) for the north Pacific Plate ($a = 125$ km, $k = 3.14\ \mathrm{W\,K^{-1}\,m^{-1}}$, $\alpha = 3.28 \times 10^{-5}\ \mathrm{K^{-1}}$, $\rho = 3330\ \mathrm{kg\,m^{-3}}$, and $C_P = 1200\ \mathrm{J\,K^{-1}\,kg^{-1}}$), and a constant background mantle potential temperature of 1315 °C. The temperature structure of a cooling oceanic plate of age A_{trench} is taken as the temperature structure at $x = 0$, as described in §2, and the midocean ridge temperature structure is one of constant temperature $T_1 = 1369$ °C. Excluding the Peruvian region (symbol $\oplus$), results using this set of parameters are consistent with deepest seismogenic temperatures less than ~ 900 °C. The equivalent modelled potential temperature $T_{p,d}$ above which deep and intermediate-depth earthquakes do not occur is ~ 750 °C.

[Fig. 4 about here.]

Figure 5 shows that, when the physical parameters are allowed to vary with temperature as described by McKenzie et al. (2005), the modelled deepest seismogenic temperatures are significantly lower than in the case of constant k, α, ρ, and C_P (Figs 2 and 4). As above, the temperature structure of a cooling oceanic plate of age A_{trench} is taken as the temperature structure at $x = 0$ in the subducting plate. However, the midocean ridge thermal structure is calculated from mantle decompression melting at constant entropy. This choice of ridge thermal structure typically has a small effect on modelled temperatures in the subducting plate (Fig. 2(ii)). Despite both a thinner plate (106 km, from the best-fitting model of McKenzie et al., 2005) and the hotter background mantle temperature profile resulting from the dependence of α and C_P on temperature, the results shown in Fig. 5 are consistent with deepest seismogenic temperatures less than ~ 700 °C. Equivalent potential temperatures $T_{p,d}$ for this set of modelling parameters are shown in Fig. 6, which suggests that, apart

from two regions, the deepest modelled seismogenic potential temperature are everywhere compatible with being less than $\sim 570\,^{\circ}$C. Variations in modelled plate thickness of $\pm 10\,\%$ change the modelled temperatures at the depths of the deepest earthquakes by less than $^{-15}_{+30}\,^{\circ}$C for all of the results shown, and the equivalent potential temperatures by less than $^{-15}_{+25}\,^{\circ}$C. These comparisons and general trends ignore results from the Peruvian ($\oplus$) and Pampean ($\odot$) regions, discussed separately. From the results shown in Figs 5 and 6, a limiting modelled potential temperature of $\sim 570\ ^{\circ}$C for seismogenic behaviour seem to be an overestimate at deeper values of z_d. However, the trend is more apparent when an attempt is made to account for the variation in the age of material entering the trench (Fig. 7).

[Fig. 5 about here.]

[Fig. 6 about here.]

The deepest seismogenic temperatures and potential temperatures summarised in Table 1 and plotted in Figs 5 and 6 include the effect of allowing the mantle outside the subducting slab to cool conductively (§2). This reduces the modelled temperatures at the depths of the deepest earthquakes by an average of $\sim 63\,^{\circ}$C and potential temperatures by an average of $\sim 56\,^{\circ}$C, compared to the case where the mantle outside the plate is held at a constant potential temperature of $1315\,^{\circ}$C.

Figure 7 presents estimates of deepest seismogenic potential temperatures for the same set of parameters used to produce the results in Fig. 6, with the exception that the age of material entering the trench has age A_{tip}, instead of A_{trench}. Values of A_{tip}, including uncertainties, were estimated using Eq. 8. For ocean floor whose age does not vary monotonically away from the trench,

estimates of A_{tip} using Eq. 8 are somewhat uncertain, and this uncertainty is typically larger for longer slabs (larger values of L), which are associated with deeper values of z_d. Results are omitted from Fig. 7 if the difference between maximum and minimum modelled potential temperatures exceeds 300 °C. All omitted results are consistent with deepest seismogenic potential temperatures less than ~ 570 °C. Figures 6 and 7 are plotted on the same axes, and for most profiles show slightly higher calculated potential temperatures when $A = A_{tip}$ instead of $A = A_{trench}$. This difference occurs because, for most profiles, the measured value of A_{trench} exceeds the estimate of A_{tip} from Eq. 8 (Table 1). Of the results determined using $A = A_{tip}$ not discussed separately (Peru, Pampea), two regions (northern and southern Chile) contain earthquakes in material having modelled potential temperatures in excess of ~ 570 °C. One of these results comes from a single profile in northern Chile with $z_d = 283$ km, where the two deepest earthquakes occurred in an isolated region ~ 100 km down-dip of the shallower, continuous tongue of seismicity. It is possible that these two events occurred within a recently detached portion of subducting lithosphere, for which the model used here is not accurate. The other two results come from profiles in southern Chile ($z_d = 156$ km), where the slab is relatively short (Table 1) and temperatures are likely to be significantly affected by the presence of the overriding plate, an effect not accounted for here. Only results from the Peruvian and Pampean regions are not consistent with modelled deepest seismogenic potential temperatures less than ~ 600 °C.

[Fig. 7 about here.]

Figure 8 shows the deepest seismogenic potential temperatures for results of class 2. Where significant backarc spreading is present in a region, results for each profile are plotted twice. Results shown as solid black symbols include

the effects of backarc spreading; equivalent open symbols exclude it. As discussed below, considering uncertainties in modelled plate ages and convergence rates, as well as approximations made in the thermal model employed here, there is little convincing evidence to suggest that deep and intermediate-depth earthquakes occur in subducting lithosphere having a potential temperature in excess of ~ 570–$600\,^{\circ}\mathrm{C}$.

[Fig. 8 about here.]

In order to assess whether a limiting homologous temperature governs the extent of seismogenic behaviour in subducting slabs, the class 1 deepest seismogenic temperatures shown in Fig. 5 (which uses $A = A_{trench}$ as the age of material at $x = 0$) were converted to deepest seismogenic homologous temperatures, $\Theta_{ZH,d}$, using the solidus temperature parametrisation determined by Zhang and Herzberg (1994) for dry peridotite. These values of $\Theta_{ZH,d}$ are shown in Fig. 9 (black points), along with values determined using temperatures modelled in the same way, but with an age $A = A_{tip}$ (Eq. 8) for material entering the trench (grey points). The majority of modelled values for $\Theta_{ZH,d}$ are consistent with limiting homologous temperatures for seismogenic behaviour in the range 0.31–0.42, irrespective of whether the age of material entering the trench is modelled to be A_{trench} or A_{tip}. All of the modelled homologous temperatures shown in Fig. 9 not consistent with a value of $\Theta_{ZH,d} \lesssim 0.42$ occur in areas of the South American subduction zone where the dip of the subducting slab is shallow ($\delta \lesssim 30^{\circ}$).

[Fig. 9 about here.]

5 Discussion

5.1 Class 1 results

McKenzie et al. (2005) showed that the temperature dependence of thermal conductivity k has a significant effect on the thermal structure of cooling oceanic lithosphere. Figures 2, 4, and 5 show that this temperature dependence also has a significant effect on temperatures in subducting lithospheric slabs. Thermal modelling of slabs (§2) using physical constants determined by Parsons and Sclater (1977) suggests earthquakes occur at temperatures up to $\sim 900\,^{\circ}\mathrm{C}$ (Fig. 4); with that set of modelling parameters, the modelled temperatures for earthquakes are consistent with seismogenic behaviour limited to potential temperatures $\lesssim 750\,^{\circ}\mathrm{C}$. When the temperature dependence of the relevant physical parameters is taken into account, the seismicity is instead estimated to occur at potential temperatures up to ~ 570–$600\,^{\circ}\mathrm{C}$ (Figs 6 and 7).

If the depth to which seismicity occurs in a subducting slab is governed by a limiting *potential* temperature, as opposed to temperature alone, the implication is that pressure (P) plays a role in controlling earthquake depths (Molnar et al., 1979). Cessation of seismicity presumably occurs when a transition occurs from brittle, teleseismically-recordable seismogenic behaviour to aseismic creep. The pressure dependence of the deviatoric stress σ_c required for this transition is typically expressed in terms of an activation volume $V^\star$, with $\sigma_c \propto \exp\left[\left(E^\star + PV^\star\right)/RT\right]$, where $E^\star$ is the creep activation energy, R is the gas constant, and T is the absolute (Kelvin) temperature. The approximate increase in the deepest seismogenic temperature T_d with increasing depth z_d to the deepest earthquake seen in Fig. 5 is equivalent to an activation volume

of $\sim 3(4)$ cm^{3}mol^{-1}, assuming an activation energy appropriate for dislocation creep in wet (dry) olivine of 470(540) kJmol^{-1} (Karato and Wu, 1993; Mei and Kohlstedt, 2000). The scatter in the T_d trend is considerable, and as a result the activation volume estimate is poorly constrained. The range of values permitted by the data is, however, in agreement with laboratory estimates of $V^\star$ (e.g. Hirth and Kohlstedt, 2003).

The distribution of seismogenic behaviour in subducting slabs can in the majority of cases be equally well described by a limiting *homologous* temperature between 0.31–0.42 (Fig. 9), if it is assumed that the earthquakes occur in dry peridotite with a melting temperature equal to the solidus temperature as parametrised by Zhang and Herzberg (1994). Of the deepest seismogenic homologous temperatures determined from modelling using either $A = A_{trench}$ or $A = A_{tip}$, only results from a few profiles in Fig. 3 are not consistent with this limiting range, all of which are from the South American subduction zone. Ignoring results from Peru and Pampea (discussed below), these outlying profiles are either from northern Chile, where both the subducting slab descends with a very shallow dip ($\delta \approx 15°$) and the deepest earthquakes may occur in detached slab material, or from southern Chile, where the slab dips at a moderately shallow angle and is relatively short ($\delta \approx 28°$, $L_{max} \approx 340$ km). In each situation, the cooling effect of the overriding plate is probably significant.

In much the same way as the dependence of a critical deviatoric stress σ_c on pressure can account for a potential temperature limit to seismogenic behaviour, a corresponding limiting homologous temperature can be explained by the temperature dependence of the creep activation enthalpy $H^\star \equiv E^\star + PV^\star$. For a variety of materials with absolute melting temperature $T_{m,abs}$, the ratio $H^\star/T_{m,abs}$ is approximately constant (e.g. Weertman and Weertman,

1975). It follows that the ratio of activation enthalpy to absolute temperature, $H^\star/T_{abs}$, is inversely proportional to the homologous temperature. Any transition from seismic to aseismic behaviour at a constant value of $H^\star/T_{abs}$ thus appears to take place at a roughly constant homologous temperature.

The governance of subduction zone seismicity by some critical, depth dependent temperature is not a new concept. As mentioned above, work by Molnar et al. (1979) extended the analysis of McKenzie (1969, 1970) to several subduction zones and concluded that seismicity is everywhere limited to material with potential temperatures less than $\sim 630\,^\circ$C. Wortel and Vlaar (1988) used the technique of Wortel (1982) to analyse temperatures and seismicity in descending slabs to show that the subduction zone earthquakes occur in material having homologous temperatures up to $\Theta = 0.54 \pm 0.04$. Using a temperature-dependent conductivity (Hofmeister, 1999; Schatz and Simmons, 1972), the improved earthquake locations provided by the updated catalogue of Engdahl et al. (1998), and more recent estimates of mantle melting temperature (Zhang and Herzberg, 1994), this study suggests the same qualitative conclusions as Molnar et al. (1979) and Wortel and Vlaar (1988), but that the limit on seismogenic behaviour is either a potential temperature of $\sim$ 570–600 °C, or a homologous temperature in the range $\sim$ 0.31–0.42. Of course, computed values of homologous temperature depend strongly on the melting temperature T_m of the subducting material. To compute values of Θ, Wortel and Vlaar (1988) used values of T_m calculated by Stacey (1977), which, in the depth range of interest, are $\sim$ 100–300 °C lower than the values used in this study. The deepest seismogenic temperatures calculated here yield a critical homologous temperature for seismicity at depths $\lesssim$ 450 km of $\Theta_{Stacey,d} \approx 0.35$–$0.50$ when compared with Stacey's melting temperatures, but the deeper events (depths

$\gtrsim$ 450 km) appear to be limited to lower values of $\Theta_{Stacey,d} \approx 0.35$–$0.43$. Owing to the effects on mantle melting point of composition (e.g. Hirschmann, 2000) and water content (e.g. Inoue, 1994), it is difficult to know the melting temperature accurately without detailed knowledge of composition and the proportion of hydrous phases in subduction zones up to depths $\sim$ 670 km. To avoid this complication, the characterisation of the depth dependence of seismogenic behaviour in terms of a limiting potential temperature is preferred over that using homologous temperature, in light of the comparable fit to the data that the two descriptions provide (Figs 6, 7, and 9).

The above discussion ignores results from the Peruvian and Pampean regions. These are the only class 1 regions containing earthquakes inconsistent with modelled deepest seismogenic potential temperatures $\lesssim$ 570–600 °C (Figs 6 and 7). The seismicity in these regions indicates that the Nazca Plate subducts subhorizontally (e.g. Engdahl et al., 1998; Grange et al., 1984; Gutscher et al., 2000; Hasegawa and Sacks, 1981). A subhorizontally subducting plate maintains thermal contact with the overriding South American Plate, which is cooler than the asthenospheric mantle. Consequently, the subducting plate remains relatively cold, and models assuming the mantle surrounding this plate to be as hot as the asthenosphere (such as the one employed here) will overestimate the slab temperature structure. This explains the high potential temperatures modelled here for the seismicity in the subducting Nazca plate (Emmerson, in prep.). The same effect, perhaps occurring to a lesser extent, can account for the relatively high temperatures modelled for profiles from other parts of the South American subduction zone where the dip of the slab is moderately shallow.

In the thermal modelling employed here, inclusion of a temperature-dependent

conductivity significantly reduces the estimated temperatures in subducting slabs compared to previous studies (Fig. 2). The experimental data on which the parametrisation of conductivity used here is based (Hofmeister, 1999; McKenzie et al., 2005) were published over 35 years ago by Schatz and Simmons (1972), and as such have been available to those earlier studies. Wortel (1982) used the data of Schatz and Simmons to test the effects of a temperature-dependent conductivity on temperature, and found that dependence to yield "solutions which very closely agree with those for a constant diffusivity $\kappa = 0.9\times10^{-6}\ \mathrm{m^2\,s^{-1}}$." Such a result is confusing for two reasons. First, while for a narrow range of subduction zones having similar subduction parameters (plate age, convergence rate, dip) it may be possible to match results from modelling with constant physical parameters to results using temperature-dependent ones through a judicious choice of the diffusivity, it is difficult to see how the same choice of diffusivity can apply for all subduction zones studied, given the resulting variations in thermal structure between subduction zones and the strong variation of κ with temperature (resulting mainly from the temperature dependence of conductivity k). Secondly, the choice of $\kappa = 0.9 \times 10^{-6}\ \mathrm{m^2\,s^{-1}}$ seems rather high to match the results using temperature-dependent parameters. Although the values of k, ρ, and C_P determined by Parsons and Sclater (1977) yield a diffusivity of $\kappa = 0.79 \times 10^{-6}\ \mathrm{m^2\,s^{-1}}$, the average value of the temperature-dependent diffusivity resulting from the computed temperatures within the plate region ($0 \leqslant y \leqslant 106$ km) of Fig. 2(ii) is notably lower, with a value of $\kappa = 0.56 \times 10^{-6}\ \mathrm{m^2\,s^{-1}}$. Of the class 1 profiles analysed in this study, half have both values of $A_{trench} = 50 \pm 25$ Myr and convergence rates $v_\perp = 75 \pm 25\ \mathrm{mm\,yr^{-1}}$; values of $A_{trench} = 50$ Myr and $v_\perp = 75\ \mathrm{mm\,yr^{-1}}$ were used to compute the thermal structures shown in Fig. 2. There is little evidence from the results presented in §4 to suggest that

the effects of a temperature-dependent conductivity, as parametrised from the results of Schatz and Simmons (1972), can be accounted for using a constant diffusivity of $\kappa = 0.9 \times 10^{-6}$ m^2 s^{-1}.

5.2 Class 2 results

With the exception of the Aegean, class 2 regions are so categorised because of poorly known variations in their convergence rates over the past few Myr. The timescale over which velocity variations must be considered for a slab is the "descent time," defined here as the time taken for the deepest portion of the seismogenic slab to reach its current depth. This timescale is analagous to the "assimilation time" of Shiono and Sugi (1985), or the "resorption time" of Wortel and Vlaar (1988). The descent time is difficult to estimate, however, as it depends on the convergence rate. Based on present-day convergence rates and seismogenic slab lengths (Table 1), descent times for arcs bordering the Philippine Sea Plate (Bonin, Izu, Ryukyu, Mariana) vary between $\sim$ 6–20 Myr. Although the deepest earthquakes in each of these arcs are consistent with potential temperatures $\lesssim$ 570–600 °C (Fig. 8), these results are poorly constrained because of the unknown history of plate motion over such periods. In the Mariana, the relative importance of backarc spreading, compared to the effects of changes in the stable-plate relative motions on deepest seismogenic temperatures, cannot be accurately determined without a good knowledge of this history.

Backarc spreading contributes to the overall convergence rate at a plate boundary and can have a large effect on deepest seismogenic potential temperatures (Fig. 8). In general, the rate of backarc spreading varies over the descent

time. This is illustrated behind the Tonga arc, where spreading in the Lau Basin has been active for the past $\sim$ 3–6 Myr (Weissel, 1980), less than the $\sim$ 7–8 Myr descent time (based on a full spreading rate determined from magnetic anomalies by Jarrard, 1986). However, geodetic measurements yielding full spreading rates as high as $\sim$ 160 mm yr^{-1} (Bevis et al., 1995) suggest the rate of spreading has increased. Given that relative velocities between the stable interiors of the large Australian and Pacific plates are likely to have changed little over the past few Myr, changes in backarc spreading rates during this period will have dominated variations in convergence rate. For Tonga, the present spreading rate is unlikely to equal, and is probably greater than, that averaged over the descent time. The likely limits on the average convergence rates, both in Tonga and Kermadec, where backarc spreading has been active for $\sim$ 2 Myr (Malahoff et al., 1982), mean there is no strong evidence to suggest that deepest seismogenic potential temperatures in these regions exceed $\sim$ 570–600 °C. It should be noted that the modelling method used here may underestimate the deepest seismogenic potential temperatures in Tonga, as the seismogenic portion of the slab extends subhorizontally for several hundred km along the bottom of the upper mantle (e.g. Chen and Brudzinski, 2001).

The spreading rate behind the South Sandwich arc can be estimated by treating the region east of the East Scotia Ridge as a separate small plate (the Sandwich Plate), moving eastwards relative to the Scotia Plate in the west (Thomas et al., 2003). Despite the small size of the Sandwich Plate, the presence of magnetic lineations allow historical variations in the relative velocity between it and the South American Plate to be reasonably well determined. Spreading in the South Sandwich backarc has increased to its present full rate from a

full rate of $\sim$ 50–60 mm yr^{-1} $\sim$ 4 Myr ago (Barker, 1972). The present consumption rate of $\sim$ 70 mm yr^{-1} yields a descent time of $\sim$ 4 Myr, suggesting that the average rate relevant to the deepest seismicity beneath the South Sandwich Islands is that which includes the present rate of backarc spreading. Therefore, as shown in Fig. 8, the deepest seismogenic potential temperatures in this region probably lie within the 300–600 °C range (solid symbols), and not 700–1000 °C (open symbols). These relatively large variations of 300 °C in potential temperature within either set of South Sandwich results presented in Fig. 8 result from variations in the age of the subducting plate, which varies between 26–74 Myr for the profiles analysed.

Where consumption rates at subduction zones are unlikely to have remained constant over the time taken to consume the observed length of seismogenic slab, it is difficult to estimate the deepest seismogenic potential temperatures accurately. As a result, the class 2 results affected by this difficulty do not accurately constrain thermal controls on deep seismicity. However, in these cases, and in the case of the Aegean subduction zone, where the age of material entering the trench is not well known, sufficient ambiguity exists about temperatures at the depths of the deepest seismicity to leave conclusions based on the class 1 results unaffected.

5.3 Additional effects

This study has shown that potential temperatures at the depths of the deepest subduction zone earthquakes do not exceed $\sim$ 570–600 °C. The variation in temperature at these depths can be described equally well by a limiting homologous temperature for seismogenic behaviour of $\sim$ 0.42, assuming the solidus

temperature parametrisation determined by Zhang and Herzberg (1994) for dry peridotite. However, certain effects were not included in the modelling employed here. Circulating mantle in the wedge above a subducting plate is cooled conductively on contact with the overriding plate as it proceeds towards the wedge corner. There also exists a period of time $\gtrsim 1$ Myr, over which a given portion of the subducting plate is in direct contact with the relatively cold overriding one (illustrated schematically by the hachured region in Fig. 1), rather than with the hot mantle. Both of these effects decrease the average temperatures on the upper slab surface below those of the isentropic mantle. The magnitude of slab cooling through conductive contact with the overriding plate increases with decreasing dip and decreasing convergence rate. England and Wilkins (2004) use constant physical parameters and incorporate these cooling effects to some extent. Comparisons were made with their model using a constant plate thickness of 100 km, constant thermal diffusivity of $10^{-6}\,\mathrm{m^2\,s^{-1}}$, and the constant values of α and C_P employed in the present study. At down-dip distances of 600 km, England and Wilkins' model yields potential temperatures that are as much as $\sim 230\,^\circ\mathrm{C}$ lower than those produced by the model in §2 for a dip of 30° and a convergence rate of $40\,\mathrm{mm\,yr^{-1}}$. The difference is less pronounced for a dip of 60°, which produces potential temperatures that are $\sim 110\,^\circ\mathrm{C}$ lower (P. England, pers. comm., 2006). For a convergence rate of $100\,\mathrm{mm\,yr^{-1}}$, the differences are $\sim 100\,^\circ\mathrm{C}$ ($\delta = 30°$) and $\sim 60\,^\circ\mathrm{C}$ ($\delta = 60°$). As such, these results can explain the modelled temperatures incompatible with a trend whereby seismogenic behaviour is limited to material having potential temperatures $\lesssim 570$–$600\,^\circ\mathrm{C}$ or homologous temperatures $\lesssim 0.42$. All of the outlying results determined here occur for slabs with shallow dips.

Both the model in §2 and that of England and Wilkins neglect any changes in plate thickness that may occur over the time taken to subduct the seismogenic portion of a slab. Because the diffusion time for a body scales as the square of its thickness, changes in slab thickness can potentially have a large effect on its temperature structure. The magnitude of this effect can be estimated from rates of strain due to earthquakes, and is probably largest in slabs that are entirely under compression, such as the highly seismogenic Tonga-Kermadec system. Nothard et al. (1996) estimated downdip seismic shortening strain rates in the Tonga slab to be $\gtrsim 10^{-15}\,\mathrm{s}^{-1}$, which, if representative of the long-term strain in the entire slab, and if all shortening is accommodated by slab thickening, corresponds to an increase in slab thickness $\gtrsim 20\,\%$ over a ~ 7 Myr descent time. Slab thickening in subduction zones may be even greater than this (e.g. King, 2001, and references therein). The effects of cooling in the mantle wedge, cooling on contact with the overriding plate, and slab thickening all act to decrease temperatures in subducting slabs.

Temperatures in subducting slabs may be increased by several effects, however, particularly at the deeper of the earthquake depths considered here. The decrease in conductivity with temperature modelled here may not apply as modelled to slab material penetrating the wadsleyite stability field, widely accepted to occur at the 410 km seismic discontinuity. Although for olivine the increase of thermal conductivity with pressure is small compared to the decrease with temperature (Hauck et al., 1999; Hofmeister, 1999), thermal conductivities have been measured to increase by $\sim$ 30–50 % at the transition to wadsleyite (Hofmeister, 1999; Xu et al., 2004). Conductivities are also increased by radiative heat transfer (Marton et al., 2005; Xu et al., 2004), though the magnitude of this contribution is dependent on grain size and may

be small (Hofmeister, 1999). [The model of Hofmeister (1999), adapted for use here, is based on fine grain sizes. As grain size increases, the radiative contribution to conductivity increases (Hofmeister, 2005).] An increase in conductivity increases the rate of heat transfer and, consequently, temperatures within the slab. Furthermore, the transition from olivine to wadsleyite is exothermic, and could raise slab temperatures by $\sim 100\,^{\circ}\mathrm{C}$ (e.g. Turcotte and Schubert, 1971). However, quite how rapidly the slab interior is equilibrated with the surrounding mantle remains a subject of much interest (e.g. Rubie and Ross, 1994; Sung and Burns, 1976) and, like melting temperature, may be strongly affected by the amount of water present (Hosoya et al., 2005). It is possible that metastable olivine persists to depths exceeding 410 km, and therefore that conductivities, and consequently temperatures, remain relatively low in at least part of the slab. There thus remains a further problem with the choice of melting temperature from which to calculate homolgous temperatures, namely whether the equilibrium melting temperature of the mantle surrounding a subducting slab is representative of that posessed by the material contained within it. Whatever the state of the slab interior, changes in mineralogy outside the slab will, as a result of the associated changes in conductivity, almost certainly affect temperatures both outside and within the slab, but it is difficult to justify the inclusion of such changes when much uncertainty surrounds the physical parameters associated with seismogenic portions of slabs within the mantle transition zone.

The phenomena acting to lower temperatures below those modelled in this study could, in principle, apply to all subduction zones, whereas the factors that may elevate temperatures within subducting slabs above those modelled here would have the greatest effect on those subduction zones where the deep-

est seismicity lies deeper than 410 km. However, any lithospheric thickening over the descent time of the slab seems more likely in slabs penetrating to the 670 km discontinuity, which appears to be a barrier to seismogenic behaviour and, presumably, acts as a source of resistance to subducting material. Any effects of elevated conductivity across phase boundaries could thus be offset by an increase in the thermal time constant, as a result of any slab thickening. Furthermore, all modelling performed here has assumed a steady state for the subduction process, which may not apply to recently-formed subduction zones. The interplay between the effects not accounted for here requires a more detailed knowledge of descending slabs than is currently available, particularly with respect to the polymorphic state of olivine present in the slab interior, and the evolution of the slab thickness as it descends. This paper shows that, based on the currently available knowledge, the occurrence of earthquakes in subduction zones is consistent with seismogenic behaviour limited to material with a potential temperature $\lesssim$ 570–600 °C.

6 Conclusions

This paper has shown that, where plate subduction parameters are well known, there is no strong evidence for teleseismically recorded intermediate and deep focus earthquakes occurring in subducting lithosphere with a potential temperature exceeding $\sim$ 570–600 °C, or, when temperatures are compared to the solidus temperature of dry peridotite, a homologous temperature of $\sim$ 0.42. This means that almost all mantle earthquakes having a magnitude large enough for them to be recorded teleseismically occur in material with a potential temperature $\lesssim$ 600 °C, irrespective of whether that mantle material is

found in a cooling oceanic plate, beneath a continent, or in a subducting slab. The Peruvian and Pampean sections of the Nazca Plate appear to contain earthquakes occurring at unusually high potential temperatures, but the shallow dip of subduction in this region probably means that the descending slab is kept cold by the overriding South American Plate. This effect is not accounted for by the model employed here and more detailed modelling of these regions is required. The modelling summarised in the present paper has demonstrated the significant effect that temperature-dependent physical parameters have on the resulting modelled thermal structure in subducting lithosphere, compared to the analytic case where the physical parameters remain constant. The thermal conductivity, which decreases with increasing temperature, dominates this effect.

Acknowledgements

We would like to thank A. Copley, P. England, J. Jackson, and R.D. Müller for their help. The comments of two anonymous reviewers helped us to improve the manuscript. Pecuniarily, B. Emmerson would like to thank J. Jackson and the Cambridge Philosophical Society for support. This is Cambridge Earth Sciences contribution ES.8703.

References

Barker, P., 1972. A spreading centre in the east Scotia Sea. Earth Planet. Sci. Lett. 15 (2), 123–132.

Bevis, M., Taylor, F. W., Schutz, B. E., Recy, J., Isacks, B. L., Helu, S.,

Singh, R., Kendrick, E., Stowell, J., Taylor, B., Calmantli, S., March 1995. Geodetic observations of very rapid convergence and back-arc extension at the Tonga arc. Nature 374 (6519), 249–251, doi:10.1038/374249a0.

Bouhifd, M., Andrault, D., Fiquet, G., Richet, P., 1996. Thermal expansion of forsterite up to the melting point. Geophys. Res. Lett. 23 (10), 1143–1146, doi:10.1029/96GL01118.

Chen, W.-P., Brudzinski, M. R., 2001. Evidence for a large-scale remnant of subducted lithosphere beneath Fiji. Science 292, 2475–2479.

Chen, W.-P., Molnar, P., 1983. Focal depths of intracontinental and intraplate earthquakes and their implications for the thermal and mechanical properties of the lithosphere. J. Geophys. Res. 88, 4183–4214.

Davies, J., 1999. Simple analytic model for subduction zone thermal structure. Geophys. J. Int. 139 (3), 823–828, doi:10.1046/j.1365-246x.1999.00991.x.

DeMets, C., Gordon, R., Argus, D., Stein, S., Oct 1994. Effect of recent revisions to the geomagnetic time scale on estimates of current plate motions. Geophys. Res. Lett. 21 (20), 2191–2194.

DeMets, C., Jansma, P. E., Mattioli, G. S., Dixon, T. H., Farina, F., Bilham, R., Calais, E., Mann, P., Feb 2000. GPS geodetic constraints on Caribbean-North America plate motion. Geophys. Res. Lett. 27 (3), 437–440.

Emmerson, B., Jackson, J., McKenzie, D., Priestley, K., Dec 2006. Seismicity, structure and rheology of the lithosphere in the Lake Baikal region. Geophys. J. Int. 167 (3), 1233–1272, doi:10.1111/j.1365-246X.2006.03075.x.

Engdahl, E., van der Hilst, R., Buland, R., 1998. Global teleseismic earthquake relocation with improved travel times and procedures for depth determination. Bull. Seism. Soc. Amer. 88 (3), 722–743.

England, P., Engdahl, R., Thatcher, W., Feb 2004. Systematic variation in the depths of slabs beneath arc volcanoes. Geophys. J. Int. 156 (2), 377–408,

doi:10.1111/j.1365-246X.2003.02132.x.

England, P., Wilkins, C., Dec 2004. A simple analytical approximation to the temperature structure in subduction zones. Geophys. J. Int. 159 (3), 1138–1154, doi:10.1111/j.1365-246X.2004.02419.x.

Frohlich, C., 2006. Deep earthquakes. Cambridge University Press.

Grange, F., Hatzfeld, D., Cunningham, P., Molnar, P., Roecker, S. W., Gagnepain, J., Ocola, L., Rodrigues, A., Stock, J. M., Suarez, G., Jan. 1984. The configuration of the seismic zone and the downgoing slab in southern Peru. Geophys. Res. Lett. 11, 38–41.

Gutscher, M.-A., Spakman, W., Bijwaard, H., Engdahl, E. R., 2000. Geodynamics of flat subduction: Seismicity and tomographic constraints from the Andean margin. Tectonics 19, 814–833, doi:10.1029/1999TC001152.

Hasegawa, A., Sacks, I. S., Jun. 1981. Subduction of the Nazca plate beneath Peru as determined from seismic observations. J. Geophys. Res. 86, 4971–4980.

Hauck, S. I., Phillips, R., Hofmeister, A., Nov 1999. Variable conductivity: Effects on the thermal structure of subducting slabs. Geophys. Res. Lett. 26 (21), 3257–3260, doi:10.1029/1999GL010831.

Hirschmann, M., Oct 2000. Mantle solidus: experimental constraints and the effects of peridotite composition. Geochem. Geophys. Geosyst. 1, 2000GC000070, doi:10.1029/2000GC000070.

Hirth, G., Kohlstedt, D., 2003. Rheology of the upper mantle and the mantle wedge: A view from the experimentalists. In: Eiler, J. (Ed.), Inside the subduction factory. Vol. 138 of Geophysical Monographs. American Geophysical Union, Washington, D.C., pp. 83–105.

Hofmeister, A., 12 March 1999 1999. Mantle values of thermal conductivity and the geotherm from phonon lifetimes. Science 283 (5408), 1699–1706,

doi:10.1126/science.283.5408.1699.

Hofmeister, A., Aug. 2005. Dependence of diffusive radiative transfer on grain-size, temperature, and Fe-content: Implications for mantle processes. J. Geodyn. 40 (1), 51–72, doi:10.1016/j.jog.2005.06.001.

Honda, S., Yuen, D. A., 2001. Interplay of variable thermal conductivity and expansivity on the thermal structure of oceanic lithosphere. Geophys. Res. Lett. 28 (2), 351–354, doi:10.1029/2000GL012096.

Hosoya, T., Kubo, T., Ohtani, E., Sano, A., Funakoshi, K., Sep 2005. Water controls the fields of metastable olivine in cold subducting slabs. Geophys. Res. Lett. 32, L17305, doi:10.1029/2005GL023398.

Inoue, T., Sep. 1994. Effect of water on melting phase relations and melt composition in the system mg_2sio_4–$mgsio_3$–h2o up to 15 gpa. Physics of The Earth and Planetary Interiors 85 (3-4), 237–263, doi:10.1016/0031-9201(94)90116-3.

Jackson, J., Austrheim, H., McKenzie, D., Priestley, K., 2004. Metastability, mechanical strength and the support of mountain belts. Geology 32 (7), 625–628, doi:10.1130/G20397.1.

Jarrard, R., May 1986. Relations among subduction parameters. Reviews of Geophysics 24 (2), 217–284.

Karato, S.-I., Wu, P., 1993. Rheology of the upper mantle: A synthesis. Science 260, 771–778.

Kennett, J., 1982. Marine geology. Prentice-Hall.

King, S. D., Dec. 2001. Subduction zones: observations and geodynamic models. Physics of the Earth and Planetary Interiors 127 (1–4), 9–24, doi:10.1016/S0031-9201(01)00218-7.

Kojitani, H., Akaogi, M., December 1997. Melting enthalpies of mantle peridotite: calorimetric determinations in the system CaO-MgO-Al_2O_3-SiO_2 and

application to magma generation. Earth Planet. Sci. Lett. 153, 209–222.

Le Pichon, X., Chamot-Rooke, N., Lallemant, S., Noomen, R., Veis, G., July 1995. Geodetic determination of the kinematics of central Greece with respect to Europe: Implications for eastern Mediterranean tectonics. J. Geophys. Res. 100 (B7), 12675–12690.

Maggi, A., Jackson, J., McKenzie, D., Priestley, K., 2000a. Earthquake focal depths, effective elastic thickness, and the strength of the continental lithosphere. Geology 28, 495–498, doi:10.1130/0091-7613(2000)28¡495:EFDEET¿2.0.CO;2.

Maggi, A., Jackson, J., Priestley, K., Baker, C., Dec. 2000b. A re-assessment of focal depth distributions in southern Iran, the Tien Shan and northern India: do earthquakes really occur in the continental mantle? Geophys. J. Int. 143 (3), 629–661, doi:10.1046/j.1365-246X.2000.00254.x.

Malahoff, A., Feden, R., Fleming, H., May 1982. Magnetic anomalies and tectonic fabric of marginal basins north of New Zealand. J. Geophys. Res. 87, 4109–4125.

Marton, F., Shankland, T., Rubie, D., Xu, Y., March 2005. Effects of variable thermal conductivity on the mineralogy of subducting slabs and implications for mechanisms of deep earthquakes. Physics of the Earth and Planetary Interiors 149 (1–2), 53–64, doi:10.1016/j.pepi.2004.08.026.

McKenzie, D., 1967. Some remarks on heat flow and gravity anomalies. J. Geophys. Res. 72 (24), 6261–6273.

McKenzie, D., 1969. Speculations on the consequences and causes of plate motions. Geophys. J. R. Astr. Soc. 18, 1–32.

McKenzie, D., 1970. Temperature and potential temperature beneath island arcs. Tectonophysics 10, 357–366.

McKenzie, D., Bickle, M., 1988. The volume and composition of melt generated

by extension of the lithosphere. Journal of Petrology 29 (3), 625–679.

McKenzie, D., Jackson, J., Priestley, K., 2005. Thermal structure of oceanic and continental lithosphere. Earth Planet. Sci. Lett. 233 (3–4), 337–349, doi:10.1016/j.epsl.2005.02.005.

Mei, S., Kohlstedt, D., sep 2000. Influence of water on plastic deformation of olivine aggregates 2. dislocation creep regime. J. Geophys. Res. 105, 21471–21482, doi:10.1029/2000JB900180.

Mitra, S., Priestley, K., Bhattacharyya, A., Gaur, V., January 2005. Crustal structure and earthquake focal depths beneath northeastern India and southern Tibet. Geophys. J. Int. 160 (1), 227–248, doi:10.1111/j.1365-246X.2004.02470.x.

Molnar, P., Freedman, D., Shih, J., 1979. Lengths of intermediate and deep seismic zones and temperatures in downgoing slabs of lithosphere. Geophys. J. R. Astr. Soc. 56, 41–54.

Müller, R., Sdrolias, M., Gaina, C., 2006. Reconstructing vanished ocean basins. In: AGU Joint Assembly 23–26 May. Vol. T32A-03.

Nothard, S., Haines, J., Jackson, J., Holt, B., 1996. Distributed deformation in the subducting lithosphere at Tonga. Geophys. J. Int. 127 (2), 328–338.

Parsons, B., Sclater, J., Feb 1977. An analysis of the variation of ocean floor bathymetry and heat flow with age. J. Geophys. Res. 82 (5), 803–827.

Pertermann, M., Hofmeister, A. M., Nov. 2006. Thermal diffusivity of olivine-group minerals at high temperature. American Mineralogist 91 (11–12), 1747–1760, doi:10.2138/am.2006.2105.

Press, W., Teukolsky, S., Vetterling, W., Flannery, B., 1992. Numerical Recipes in FORTRAN 77: The art of scientific computing. Cambridge University Press New York.

Priestley, K., McKenzie, D., Apr 2006. The thermal structure of the litho-

sphere from shear wave velocities. Earth Planet. Sci. Lett. 244 (1–2), 285–301, doi:10.1016/j.epsl.2006.01.008.

Rubie, D. C., Ross, C. R., Oct. 1994. Kinetics of the olivine-spinel transformation in subducting lithosphere: experimental constraints and implications for deep slab processes. Physics of the Earth and Planetary Interiors 86 (1–3), 223–243, doi:10.1016/0031-9201(94)05070-8.

Schatz, J., Simmons, G., 1972. Thermal conductivity of Earth materials at high temperatures. J. Geophys. Res. 77, 6966–6983.

Sella, G., Dixon, T., Mao, A., 2002. REVEL: A model for recent plate velocities from space geodesy. J. Geophys. Res. 107 (B4), 2081, doi:10.1029/2000JB000033.

Seno, T., Stein, S., Gripp, A., Oct 1993. A model for the motion of the Philippine Sea plate consistent with NUVEL-1 and geological data. J. Geophys. Res. 98 (B10), 17941–17948.

Shiono, K., Sugi, N., Mar. 1985. Life of an oceanic plate: Cooling time and assimilation time. Tectonophysics 112 (1–4), 35–50, doi:10.1016/0040-1951(85)90171-4.

Stacey, F. D., Dec. 1977. A thermal model of the earth. Physics of the Earth and Planetary Interiors 15 (4), 341–348, doi:10.1016/0031-9201(77)90096-6.

Sung, C.-M., Burns, R. G., Mar. 1976. Kinetics of high-pressure phase transformations: Implications to the evolution of the olivine → spinel transition in the downgoing lithosphere and its consequences on the dynamics of the mantle. Tectonophysics 31 (1-2), 1–32, doi:10.1016/0040-1951(76)90165-7.

Thomas, C., Livermore, R., Pollitz, F., 2003. Motion of the Scotia Sea plates. Geophys. J. Int. 155 (3), 789–804, doi:10.1111/j.1365-246X.2003.02069.x.

Turcotte, D., Schubert, G., Nov 1971. Structure of the olivine-spinel phase boundary in the descending lithosphere. J. Geophys. Res. 76 (32), 7980–

7987.

van Keken, P., Oct 2003. The structure and dynamics of the mantle wedge. Earth Planet. Sci. Lett. 215 (3–4), 328–338, doi:10.1016/S0012-821X(03)00460-6.

Weertman, J., Weertman, J. R., 1975. High temperature creep of rock and mantle viscosity. Ann. Rev. Earth Planet. Sci. 3 (1), 293–315, doi:10.1146/annurev.ea.03.050175.001453.

Weissel, J., 1980. Evolution of the Lau Basin by the growth of small plates. In: Talwani, M., Pitman III, W. (Eds.), Island Arcs, Deep Sea Trenches, and Back-Arc Basins, Maurice Ewing Ser. vol. 1. AGU, Washington DC, pp. 429–436.

White, R., McKenzie, D., O'Nions, R., Dec 1992. Oceanic crustal thickness from seismic measurements and rare earth element inversions. J. Geophys. Res. 97 (B13), 19683–19715.

Wiens, D., Stein, S., August 1983. Age dependence of oceanic intraplate seismicity and implications for lithospheric evolution. J. Geophys. Res. 88 (8), 6455–6468.

Wortel, M. J. R., Vlaar, N. J., 1988. Subduction zone seismicity and the thermo-mechanical evolution of downgoing lithosphere. Pure and Applied Geophysics 128, 625–659, doi:10.1007/BF00874551.

Wortel, R., Apr. 1982. Seismicity and rheology of subducted slabs. Nature 296 (5857), 553–556, doi:10.1038/296553a0.

Xu, Y., Shankland, T., Linhardt, S., Rubie, D., Langenhorst, F., Klasinski, K., 2004. Thermal diffusivity and conductivity of olivine, wadsleyite and ringwoodite to 20 GPa and 1373 K. Physics of the Earth and Planetary Interiors 143, 321–336, doi:10.1016/j.pepi.2004.03.005.

Zhang, J., Herzberg, C., Sep 1994. Melting experiments on anhydrous peri-

dotite KLB-1 from 5.0 to 22.5 GPa. J. Geophys. Res. 99, 17729–17742.

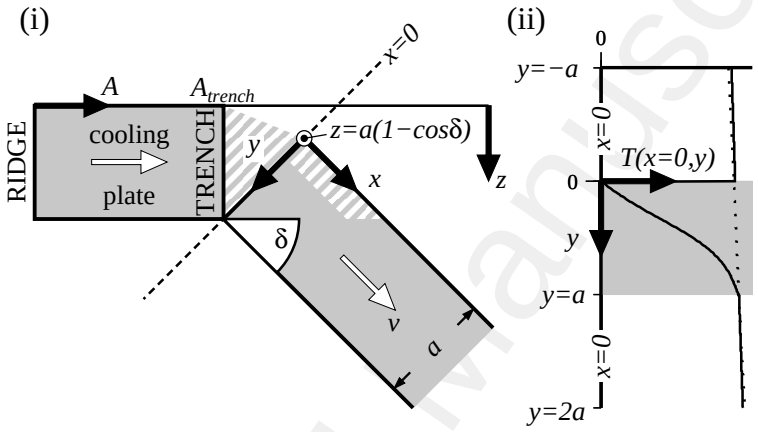

Fig. 1. (i) Model used to calculate the variation of temperature $T(x, y)$ with down-dip distance x for a slab having dip δ and thickness a; (ii) The temperature structure $T(0, y)$ of a slab with age $A_{trench} = 50$ Myr entering the trench, calculated using the plate-cooling model of McKenzie et al. (2005).

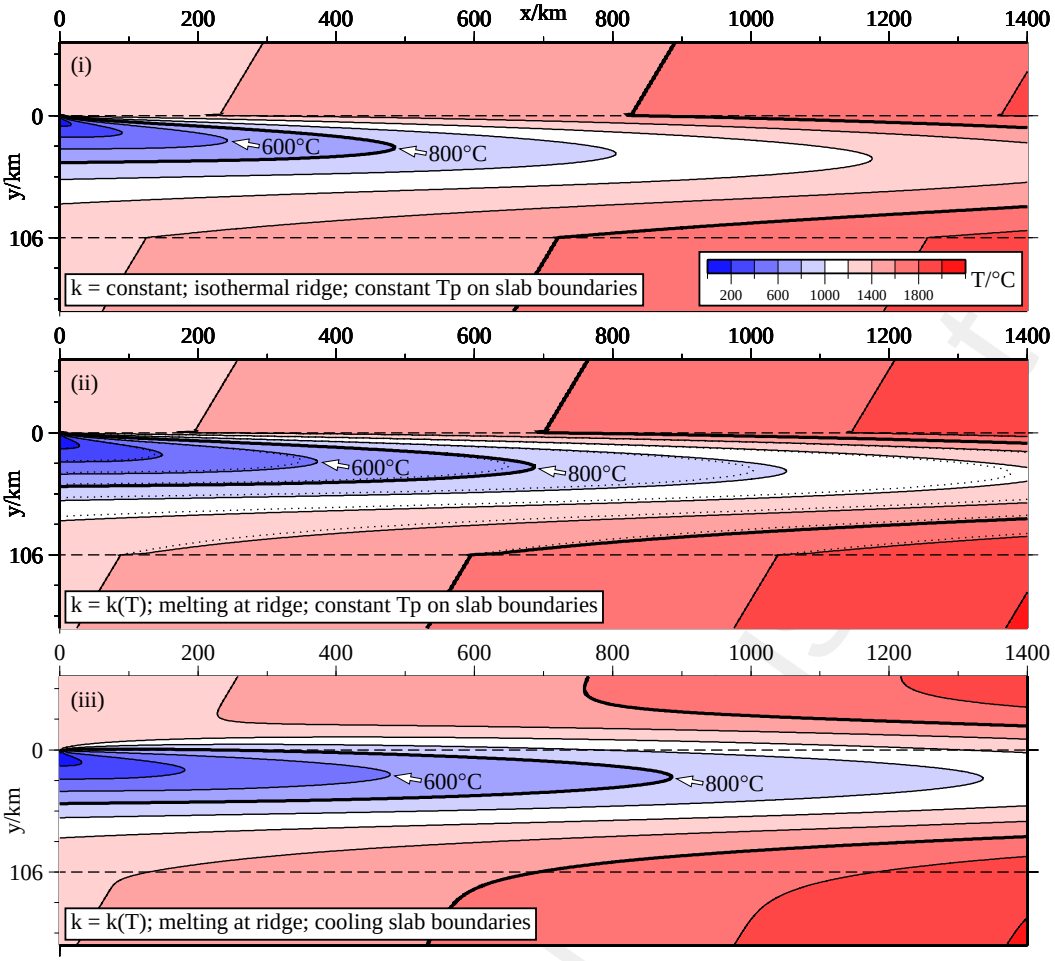

Fig. 2. Temperature contours in the (x, y) coordinate system (Fig. 1(i)) for material entering the trench at an arc-perpendicular convergence rate $v_\perp = 75$ mm yr^{-1}, with an age $A_{trench} = 50$ Myr. Celsius temperatures are contoured every 200 °C and intervals are coloured according to the inset scale; the 800 and 1600 °C contours are shown in bold. (i) Isotherms calculated using $k = 3.14$ W K^{-1} m^{-1}, $\alpha = 3.28 \times 10^{-5}$K^{-1}, $\rho = 3330$ kg m^{-3}, and $C_P = 1200$ J K^{-1} kg^{-1}, after Parsons and Sclater (1977). Although Parsons and Sclater used an oceanic plate thickness of 125 km and a temperature $T_1 = 1333$ °C at the base of the plate, the model for the subducting plate shown here has $a = 106$ km and $T_p = 1315$ °C, for comparison with Figs (ii) and (iii). The upper and lower boundaries of the subducting plate are fixed at this potential temperature and the ridge temperature structure used for the oceanic plate was one of constant temperature $T = 1361$ °C, except for the topmost element ($T = 0$ °C). (ii) Isotherms modelled using $k = k(T)$, $\alpha = \alpha(T)$, $\rho = \rho(T)$, and $C_P = C_P(T)$ are shown as solid lines. As with (i), T_p is fixed at 1315 °C on $y = 0, a$. The temperature structure at the midocean ridge was calculated as in McKenzie et al. (2005) using expressions for isentropic upwelling and melting from McKenzie and Bickle (1988). The cooler temperature structure that $\kappa = \kappa(T)$ produces in the subducting plate is clearly shown by the greater down-dip penetration of the 600 and 800 °C isotherms, as compared with (i). Dotted lines show isotherms for the same model, but with a constant temperature ridge structure of 1361 °C. The effect of the chosen ridge temperature structure on that in the subducting slab decreases with the age of material entering the trench. (iii) As in (ii), but the mantle surrounding the subducting slab is allowed to cool conductively, which further reduces the temperature within the plate.

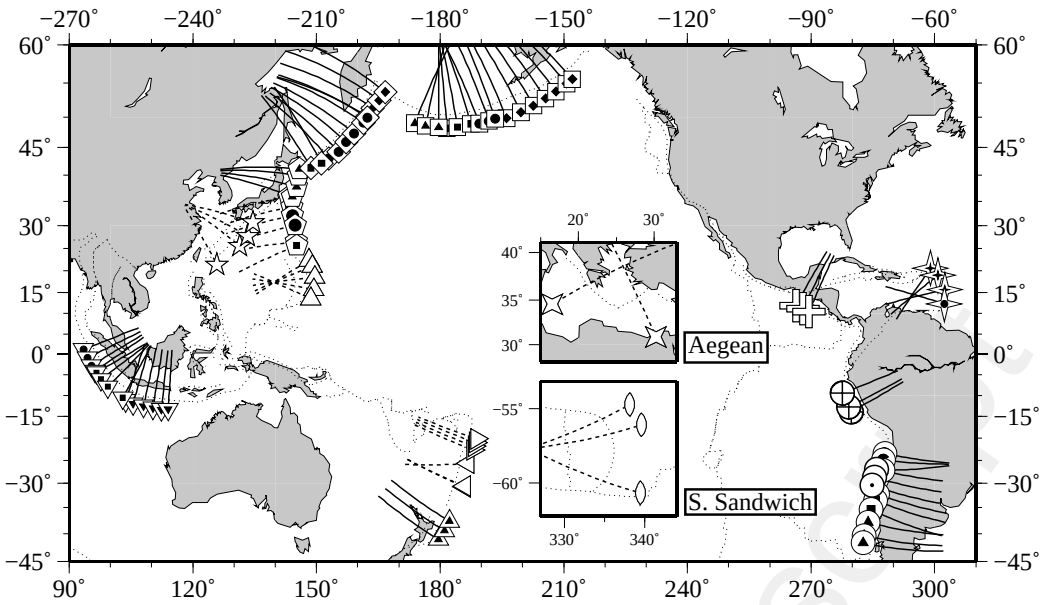

Fig. 3. Profiles of class 1 (solid lines; see §3.4) and class 2 (dashed) analysed in this study.

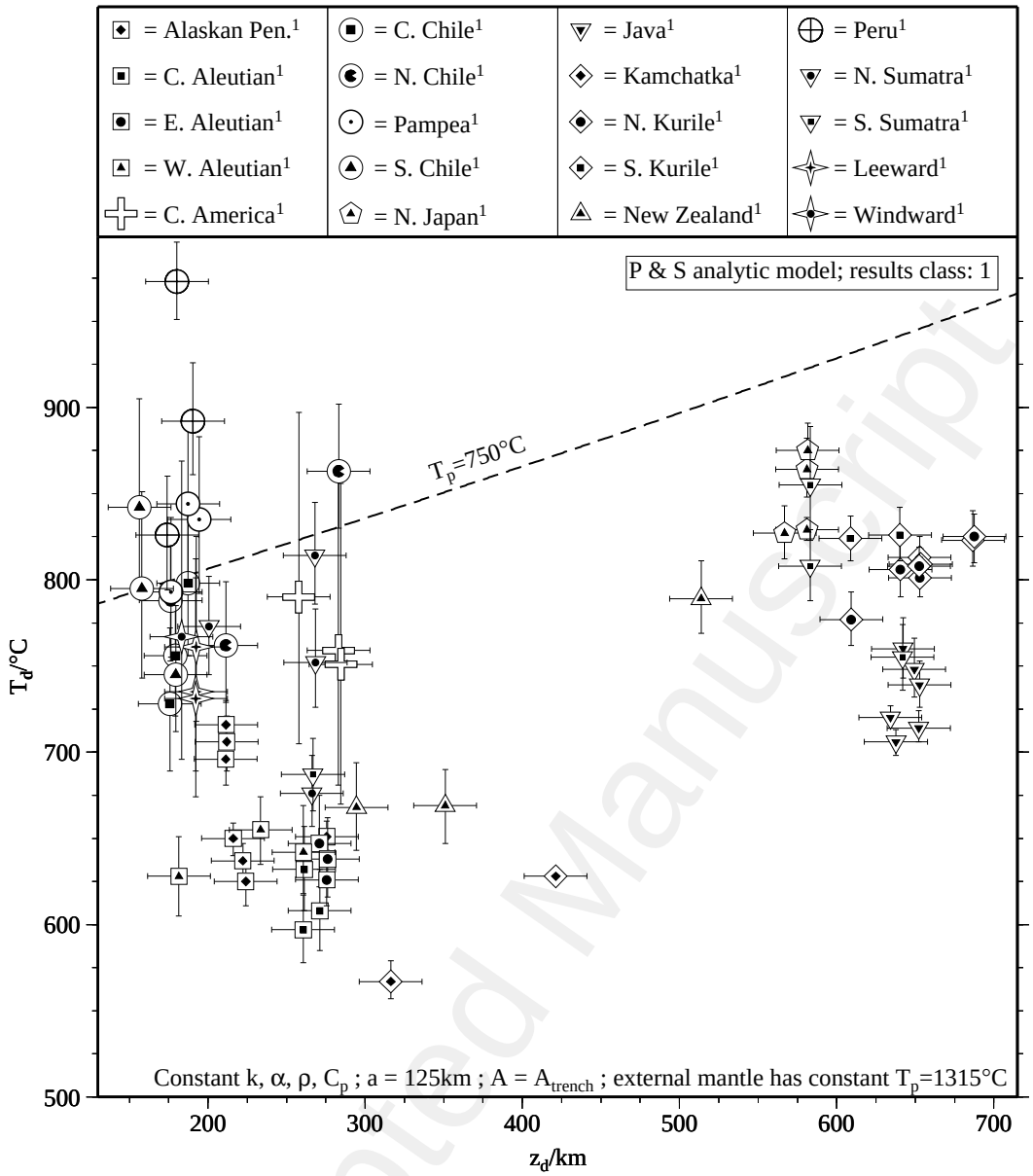

Fig. 4. Deepest seismogenic temperatures T_d as a function of depth to the deepest seismicity (z_d), for results of class 1, labelled according to the legend. Temperatures were calculated for a subducting plate having the set of constant parameters determined by Parsons and Sclater (1977). The isentropic temperature profile for a potential temperature of 750 °C is shown as a dashed line.

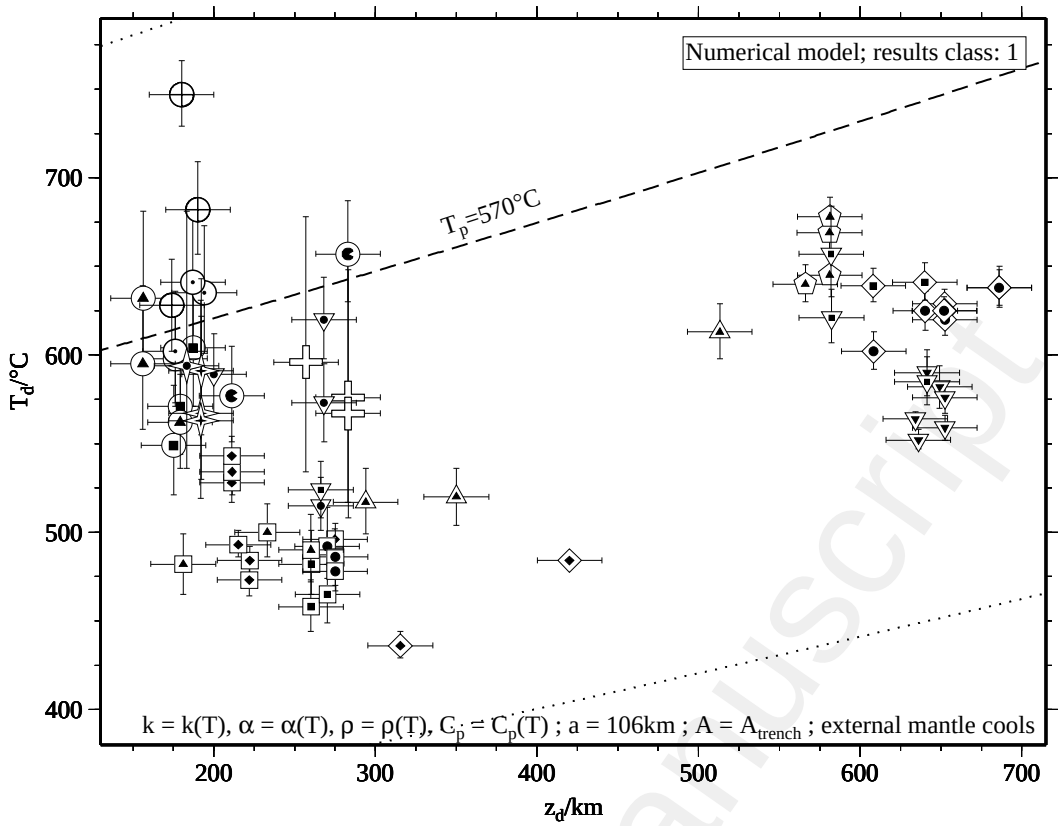

Fig. 5. As in Fig. 4, but with temperatures modelled using temperature-dependent physical parameters, and with the $T_p = 570\,^{\circ}\mathrm{C}$ isentrope labelled. Dotted lines show isentropic temperatures equivalent to the minimum and maximum potential temperatures on the vertical axis in each of Figs 6 and 7.

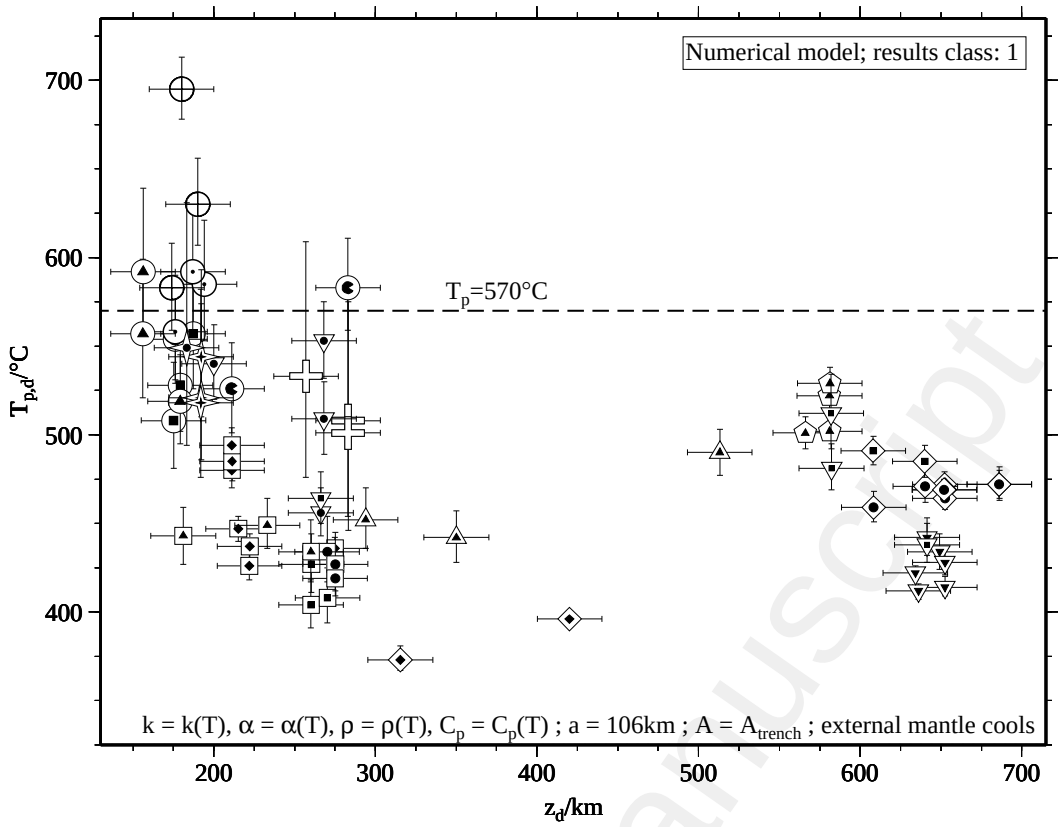

Fig. 6. Deepest seismogenic potential temperature ($T_{p,d}$) equivalents to the deepest seismogenic temperatures plotted in Fig. 5.

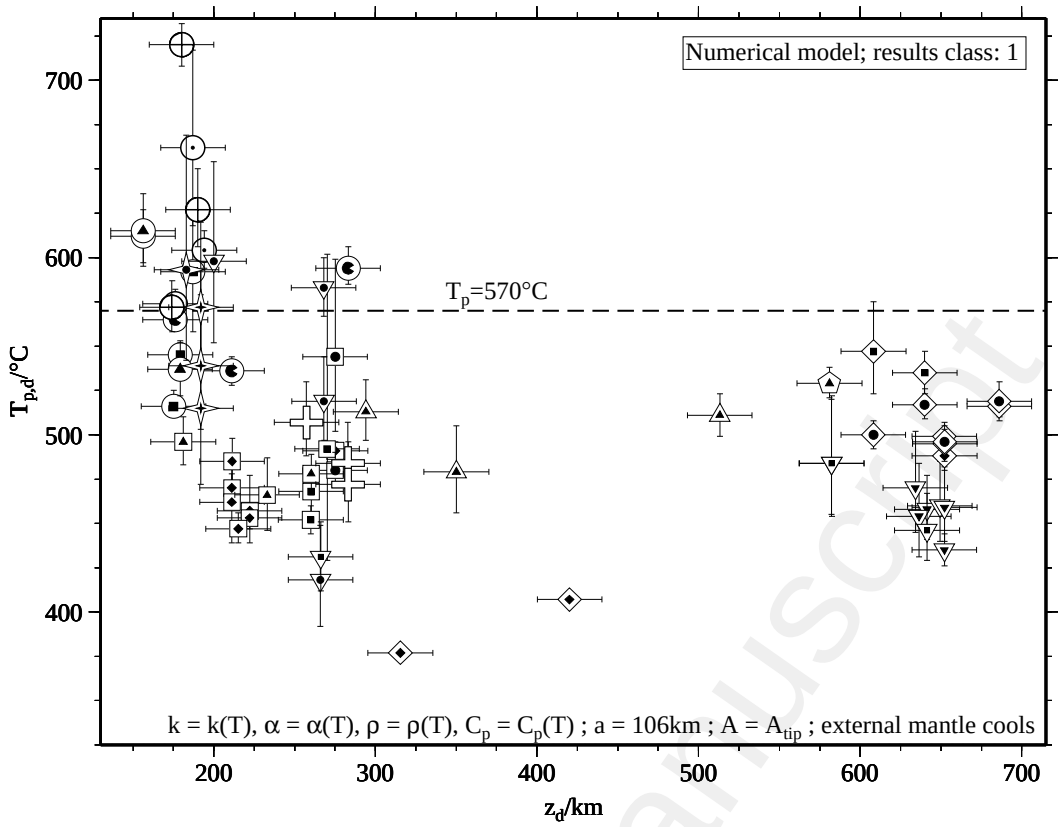

Fig. 7. Deepest seismogenic potential temperatures as in Fig. 6, but for material entering the trench with an age A_{tip} (Eq. 8) instead of A_{trench}.

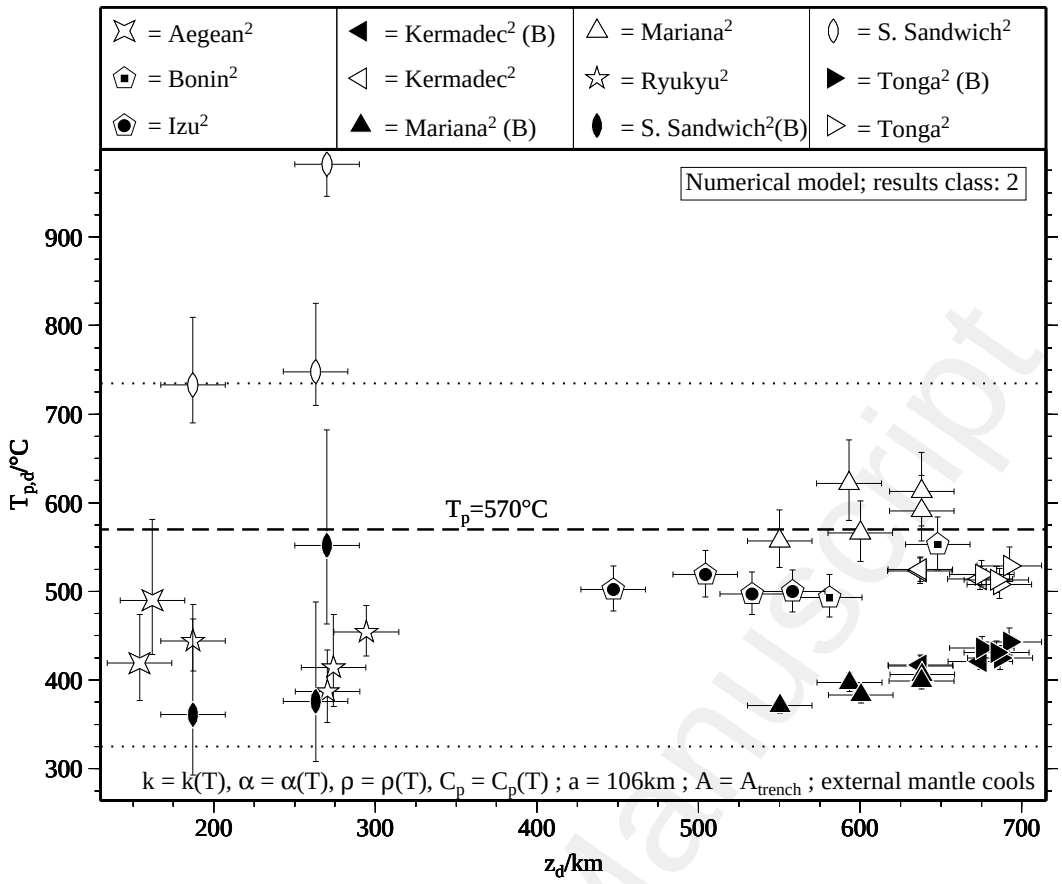

Fig. 8. Deepest seismogenic potential temperatures as in Fig. 6, but for class 2 results and plotted on an expanded scale, labelled according to the legend. For comparison, dotted lines show the limits of Figs 6 and 7.

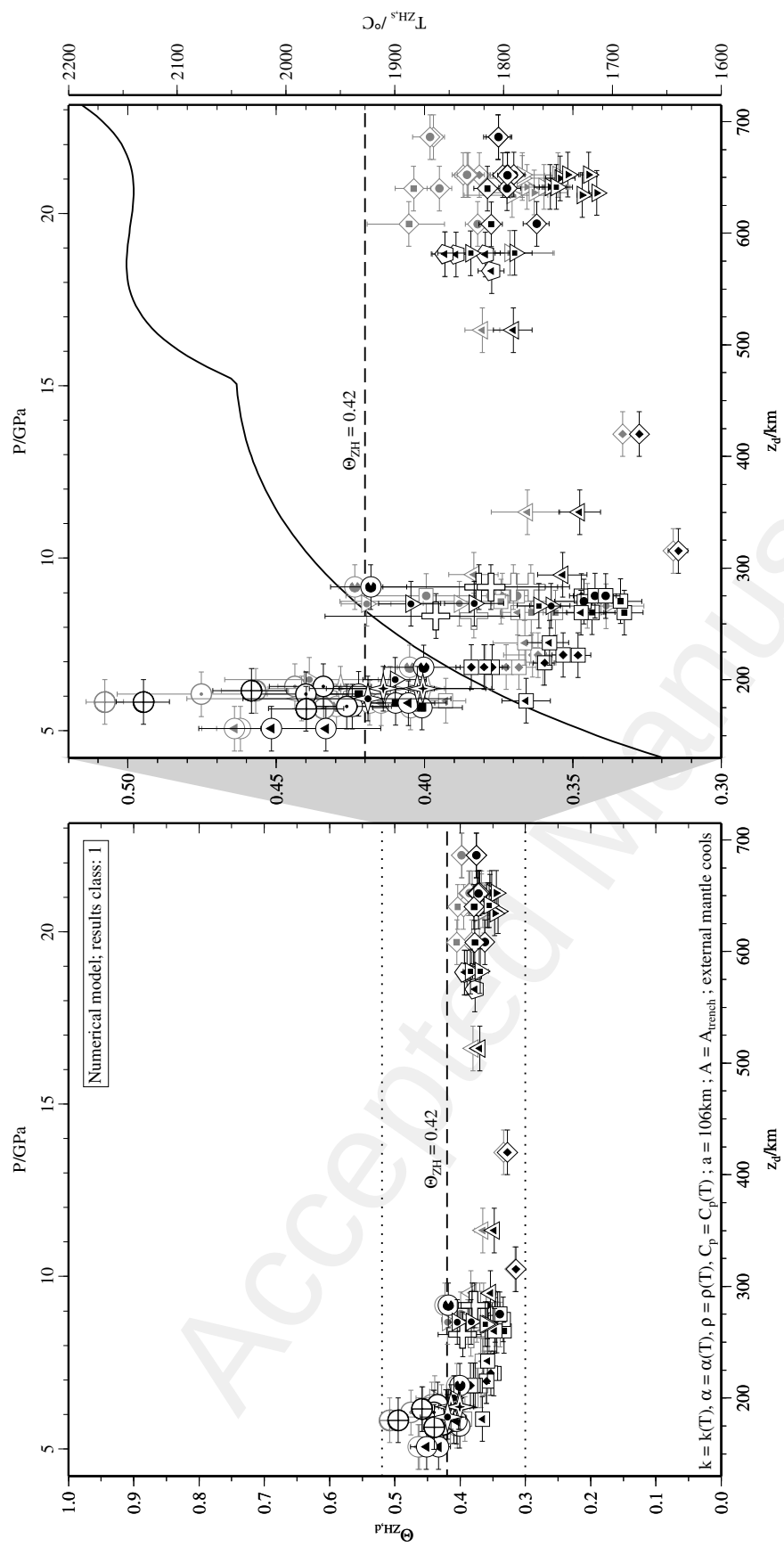

Fig. 9. Deepest homologous temperatures $\Theta_{ZH,d}$ for class 1 results, calculated using the deepest seismogenic temperatures T_d from Fig. 5 (modelled using temperature-dependent physical parameters and $A = A_{trench}$, shown here in black) and the solidus temperature $T_{ZH,d}$ shown as a solid line (see scale, right, for the range of temperatures). Solidus temperatures are from Zhang and Herzberg (1994), who performed melting experiments on anhydrous peridotite between pressures P of 5.0–22.5 GPa. Grey symbols show values of $\Theta_{ZH,d}$ calculated using values of T_d modelled using temperature-dependent physical parameters and $A = A_{hip}$. Both sets of results are plotted twice, with the left hand plot showing how the results compare to homologous temperatures between zero and unity; the plot on the right shows an expanded version of the same results. Almost all modelled deepest seismogenic homologous temperatures lie between ~ 0.31 and ~ 0.42; those exceeding the upper limit of this range are discussed in the text.

Parameters of subduction zones analysed

Region		δ	L_{max}	$v_\perp$	A_{trench}	A_{tip}	z_d	T_d/ °C	$T_{p,d}$/ °C	$\Theta_{ZH,d}$
Aegean[2]	⋈	34–38	260	16–26	120	.	154–162	451–527	419–490	0.36–0.40
Alaskan Pen.[1]	⊡	38–50	350	52–64	42–57	40–52	211–275	473–543	426–494	0.35–0.38
C. Aleutian[1]	▣	56–61	300	58–65	56–56	32–43	260–270	458–482	404–427	0.33–0.34
E. Aleutian[1]	◙	49–56	350	64–66	56–56	14–38	270–275	478–492	419–434	0.34–0.35
W. Aleutian[1]	⧈	48–56	240	31–54	56–68	42–53	181–260	482–500	434–449	0.35–0.37
Bonin[2]	⭗	76–90	600	28–35	124–144	43–121	581–648	635–726	493–553	0.38–0.41
C. America[1]	✙	52–63	320	67–74	26–27	30–32	257–283	567–596	501–533	0.38–0.40
C. Chile[1]	⦿	22–30	510	64–68	33–38	30–34	175–187	549–604	508–557	0.40–0.42
N. Chile[1]	◉	15–22	700	72–78	46–48	43–45	176–283	577–657	526–583	0.40–0.42
Pampea[1]	⊙	16–17	600	69–72	40–46	27–42	176–194	602–641	558–592	0.43–0.44
S. Chile[1]	⍟	28–31	340	73–73	18–30	16–26	156–179	562–632	519–592	0.41–0.45
Izu[2]	✹	41–60	700	38–48	111–140	49–112	447–558	610–645	497–519	0.37–0.39
N. Japan[1]	✪	28–29	1250	76–83	113–132	45–104	566–581	640–678	501–529	0.38–0.39
Java[1]	▼	62–73	850	71–73	102–128	86–101	634–652	552–590	412–442	0.34–0.36
Kamchatka[1]	◈	49–54	850	75–77	93–103	85–91	315–652	436–629	373–472	0.31–0.37
Kermadec[2] (B)	◂	51	830	110–121	90–97	75–81	637–674	558–573	416–421	0.34–0.35
Kermadec[2]	◁	51	830	56–67	90–97	75–81	637–674	686–688	514–525	0.40
N. Kurile[1]	◈	44–51	810	77–79	103–114	75–84	608–686	602–638	459–472	0.36–0.38
S. Kurile[1]	◈	39–45	980	69–70	115–120	79–80	608–640	639–641	485–491	0.38
Mariana[2] (B)	▲	85–90	720	59–65	144–153	112–136	550–638	485–546	371–406	0.31–0.34
Mariana[2]	△	85–90	720	16–22	144–153	112–136	550–638	702–795	557–622	0.40–0.44
New Zealand[1]	◬	54–63	350	32–40	110–117	71–98	294–513	517–613	442–490	0.35–0.37
Peru[1]	⊕	12–15	680	71–71	29–43	26–45	174–190	628–747	583–695	0.44–0.49
Ryukyu[2]	☆	50–54	370	61–70	32–72	38–48	187–294	442–519	387–454	0.32–0.36
S. Sandwich[2] (B)	⧫	45–52	330	65–72	26–74	46–88	187–270	397–619	361–552	0.32–0.40
S. Sandwich[2]	◊	45–52	330	5–7	26–74	0–49	187–270	789–1088	733–982	0.50–0.62
N. Sumatra[1]	▼	34–46	360	39–53	44–63	36–82	200–268	515–620	456–553	0.36–0.41
S. Sumatra[1]	▼	44–75	370	51–70	66–101	75–95	266–641	524–657	438–512	0.36–0.38
Tonga[2] (B)	▸	40–48	900	120–125	84–101	48–98	675–692	580–604	425–443	0.35–0.36
Tonga[2]	▷	40–48	900	70–75	84–101	48–98	675–692	681–710	508–529	0.39–0.40
Leeward[1]	✦	42–44	290	16–20	81–89	72–85	192–192	563–591	518–544	0.40–0.41
Windward[1]	✦	41	290	16	81	63	183	594	549	0.42

Table 1. Parameters of subduction zones analysed in this study. For each region, summary results are presented from the arc-perpendicular profiles marked by their region symbol in Fig. 3. Where ranges are given, they represent variations in values of the relevant parameter for profiles analysed in that region. δ is the dip (in °) of the seismic zone at depths exceeding 80 km, measured by eye; L_{max} is the maximum length (km) of the seismic zone determined in each region, and is also measured by eye. Mean convergence rates $v_\perp$ ($\mathrm{mm\,yr^{-1}}$) are calculated by projecting plate-relative-velocity vectors onto the relevant profile. Ages A_{trench} and A_{tip} (Eq. 8) represent respectively the ages in Myr of seafloor currently entering the trench and the estimated age of the material at the tip of the seismic zone when it first entered the trench. Deepest earthquakes from each region have depths z_d (km), and are taken from the EHB catalogue. The final three columns show mean Celsius temperatures (T_d), potential temperatures ($T_{p,d}$), and homologous temperatures ($\Theta_{ZH,d}$) at which the deepest events are estimated to occur, using the thermal model illustrated in Fig. 2(iii) and an age A_{trench} at $x = 0$. Superscript numbers denote whether the results are termed "class 1" or "class 2" (§3.4), and results including backarc spreading in the convergence rate are labelled "B."